NON-DROPLET BASED MICROFLUIDIC DEVICES FOR CALCIUM OXALATE CRYSTALLIZATION

By

ASMA OBAID

A thesis submitted to the

Graduate School-Camden

Rutgers, The State University of New Jersey

In partial fulfillment of the requirements

For the degree of Master of Science

Graduate Program in Chemistry

Written under the direction of

Dr. George Kumi

and approved by

_____

George Kumi

_____

Alex J. Roche

_____

Georgia Arbuckle-Keil

Camden, New Jersey

May 2016

THESIS ABSTRACT

Non-droplet based microfluidic devices for calcium oxalate crystallization

By

ASMA OBAID

Thesis Director:

Dr. George Kumi

Microfluidic systems provide a distinct environment to study crystallization because of their unique properties, which include their superior heat and mass transport control. While continuous flow platforms are particularly appealing for crystal synthesis because of their relative simplicity, crystal adhesion to the channel wall is routinely a problematic issue. However, appropriately configured systems can minimize this problem. To this end, a non-droplet-based system that reduces or circumvents the problematic issue of crystal adhesion during crystallization in microfluidic devices has been developed. The capabilities of this system with respect to the effect of local system parameters (*e.g.,* calcium and oxalate ion concentration, and the concentration of certain pertinent chemical species) on the calcium oxalate (CaOx) crystallization process have been examined. A variety of microscopy-based methods (including scanning electron, confocal Raman and Fourier Transform Infrared microscopy) were used to demonstrate that the dispersity in crystal size, shape and morphology increases with increasing calcium and oxalate ion input concentrations into the system. Additionally, CaOx crystals formed in high oxalate ion environments were found to be small in size when compared to those created in a calcium-rich environment. CaOx crystallization experiments involving a

variety of chemical species show that this system can readily be applied to establish the influence of specific entities on a crystallization process. Design improvements, based on the obtained results, are outlined.

Dedication

I would like to dedicate my thesis to my lovely husband MOHAMED who has sacrificed everything, including his job, time, family, and friends, to support me. His love and care have always given me strength and motivated me to do my best. Also, I dedicate my thesis to my gorgeous sons: ABDULAZIZ, ALI, OMAR, and ADI.

I dedicate this work to my precious parents (Omar and Fatimah, and my mother in-law (Al allah) who pray for our safety and success everyday. I appreciate my dad coming all the way from Saudi Arabia to visit me at school in order to see my lab and the fantastic faculty with whom I have been working.

I also dedicate my thesis to my brothers and sisters, especially Abdulelah, who has always been the greatest support in my family. Whenever I need anything, he is always the first one to help, and I thank him for that.

Final dedication to my best friend, Kelly Van Camp, who has been the best example for being a loyal friend.

Acknowledgements

First, I am grateful to Allah for helping me and making it easy for me to be at Rutgers – Camden. I also thank Allah for my well-being that was necessary to finish my studies.

Overall, I thank everyone at Rutgers – Camden for providing me this unique opportunity and supporting me academically. I quickly felt comfortable here, as my worries and fears from the first semester quickly dissipated due to the welcoming and friendly environment.

Additionally, no words can describe my gratitude and appreciation to my thesis advisor Dr. Kumi for providing and sharing his valuable knowledge. He always welcomes any idea, question or a trouble about my research and writing. I thank him for his patience and valuable comments while reviewing my thesis. His superb advice, guidance, and insightful suggestions gave me deeper insight in my research. Dr. Kumi is incredibly organized and always had great explanation for every question. Besides just the knowledge I had learned from him, his ethics, personality, and modesty have taught me so many incredible things. The time I spend working in his lab will be a time I will never forget, and I will continue to look back on it fondly for years to come.

I thank my committee members, Dr. Roche and Dr. Arbuckle, for being part of my thesis committee. Their classes provided me with valuable information and pushed me to think deeply and fully understand my project. Dr. Roche's free radical class was my favorite; his breadth of knowledge was inspiring, and the way that he explained organic chemistry made me love the subject even more than before.

The first time I met Dr. Arbuckle, I could see that she was such a kind, modest, and friendly person. She is like a mom to all of the students in the department. I love her class and how hard she works to make everyone understand, pushing her students to learn as much as possible. I will miss our conversations so much; she is an incredible woman and the best female professor I have ever had the pleasure of working.

I would also like to thank Dr. Jinglin Fu, Dr. Hao Zhu, Mrs. Jinnie Anstice, and Mr. Peter Fazzino for all of their help along the way. Many thanks to Mr. Brock Warren (the writing tutor for graduate students) for his help editing and reviewing my thesis.

Table of Contents

List of Figures

List of Tables

1. Introduction

1.1 Crystallization

Crystallization is a thermodynamically sensitive operation in which solid matter is produced from a fluid (*e.g.,* supersaturated solutions or supercooled melts).[1, 2] It is a process that occurs at the interface between two phases; a solid and liquid. The rates of nucleation and crystal growth determine the number and size of the crystals. For example, favoring growth over nucleation leads to small amounts of large uniform crystals. A low level of supersaturation induces growth over nucleation, and a higher residence time (the period of time where crystals remain within a system) also induces growth of large crystals.[3]

A crystal is a three-dimensional structure of atoms or ions arranged in a geometric pattern.[2] Larger crystals are composed of smaller identical crystalline cells that repeat in a regular pattern dictated by thermodynamic principles. Each crystalline cell can become the template for crystal formation in a process known as nucleation. Nucleation is the formation of new crystals that is followed by crystal growth via the incorporation of surrounding molecules.[1]

There are two types of nucleation, namely homogeneous and heterogeneous nucleation. Homogeneous nucleation occurs in a system that only contains the same type of particles; the crystals form around a nucleus of the same composition. However, homogeneous nucleation can also occur in a system with other type of particles as long as these other particles do not influence crystal formation. The presence of foreign particles in a system generally leads to heterogeneous nucleation where some materials are integrated into the crystals. Both homogeneous and heterogeneous nucleation are

classified as primary nucleation, which is nucleation that occurs without an assistance of attrition agents or seed crystals. However, secondary nucleation exists when crystals of the same type act as seed crystals or attrition agents at low levels of supersaturation.

Once favorable conditions for crystallization exist, the formation of crystals can occur. The appearance of the produced crystals and their sizes are significant. Crystals may have different internal arrangements that affect their appearances. Crystalline and amorphous are terms used to describe the regularity of the internal structures of molecules, either ions or atoms. The term crystalline implies a high degree of regularity within the internal arrangement, resulting in precise, external, and rigid motifs known as lattices. Conversely, amorphous crystals possess relatively low degrees of a regular internal arrangement (*e.g.,* glass).[2]

The method of bonding dictates the properties of crystals. There are four major classes of crystalline solids depending on the method of bonding: covalent, metallic, molecular and ionic. A network of covalent bonds holds together a covalent crystal (*e.g.,* diamond). Metallic crystals contain metal atoms with positive charges that are held together by metallic bonds (in a "sea of electrons"). Molecular crystals consist of discrete molecules that are connected by weak forces, such as hydrogen bonds (*e.g.,* organic compounds). Ionic crystals are made of charged ions connected by electrostatic forces in the lattice crystals and separated from different charged ions by electron density (*e.g.,* sodium chloride).

Crystals often form spontaneously in the environment, and some examples of naturally occurring crystals are stalactites, stalagmites, snowflakes, and minerals. Industrial applications of crystallization include production, purification or recovery of

solid compounds, and the products of these applications are used in many aspects of our daily life.[4] Industrially, crystallization has been optimized to achieve specific goals of crystal formation, such as creating uniform crystals of a desirable size and minimizing the formation of agglomerates and liquid impurities within the crystallization system.[3]

1.2 Historical studies of crystallization

Despite many studies on crystallization, understanding nucleation and determining the growth rate and the crystal size distribution (CSD) is still a particular challenge to scientists. Crystallization was once considered more of an art than a science, thus there was a lack of research on the matter.[2] In 1669, Nicolas Steno, a Danish anatomist and geologist conducted the first advanced scientific study of crystallography, focusing on the distinctive properties of quartz crystals.[5] His work was followed by numerous other CSD studies including those on the size distribution in a continuous crystallizer by Montillon and Badger in 1927. McCabe's 1929 CSD study and his development of the ΔL law resulted in the following conclusions:[6]

(1) There is no variability in crystal shape.

(2) There is no relationship between crystal growth and their size.

(3) The supersaturation level and relative velocity are constant.

(4) No size classification and nucleation exist.

Afterward, he realized these assumptions were not realistic and that crystals can have a variety of characteristics with respect to crystal nucleation and growth rate, temperature, supersaturation, and other gradients. These early studies paved the way for in-depth studies of crystallization that continue to this day.

Even with all this exhaustive research, technical data and parameters are scarce, and that which do exist are often contradictory and vague. For instance, different studies report different crystal growth rates for the same compound that differ by an order of size or more.[2] Some researchers are now using tools that can analyze the crystallization process while it is happening. This provides a unique opportunity to understand crystallization on an atomic level and thus provides the necessary parameters to produce consistent, reproducible results.[7, 8, 9] For instance, some studies used sensors to track the supersaturation level onsite.[10, 11, 12] One limitation of these *in situ* tools is the ability to analyze the size and number of particles during the crystallization process.[8] A study has focused on using a new technique, called focused beam reflectance measurement (FBRM) to address these limitations.[9, 13] FBRM can detect small nuclei (~400 nm) and characterize the metastable region.[13, 14] Not only that, FBRM can describe the behavior of the crystals after nucleation and also measure a chord length distribution (CLD). The CLD represents the numbers, shapes, and sizes of particles under examination. Some success has also been achieved using a loop reactor to simulate the circulation time.[15] Advanced techniques like cryo-TEM can analyze molecular-level operations and provide information about the formation of nuclei (~50 nm or larger) during the nucleation process.[7] These kinds of analytical techniques give experimental insight into how the crystallization process occurs, and this insight reveals that the majority of crystals grow through accumulation on the same existent crystallites.[8]

Once the general process of crystallization was understood, scientists began to focus on specific crystal forming processes. For solute-solvent systems, supersaturated solutions are required to cause the crystallization process. Reaching the supersaturation

level can be achieved by variety of methods: cooling the solutions, modifying the pH, evaporating a portion of the solvent, reducing solubility by adding another solvent, or by creating a chemical reaction.[1, 2, 3] During nucleation, solute molecules gather into a cluster. The cluster becomes a stable nucleus under particular conditions, such as when the cluster reaches a critical size in a supercooled or supersaturated system.[2, 4]

Understanding the thermodynamics of stability and equilibrium in a solute-solvent system can help with optimizing crystallization process.[1] As shown in Figure 1, a fluid with a temperature and solute concentration above the solubility curve (above the blue dashed line) is in a stable and unsaturated thermodynamic equilibrium area.[2, 4] Any fluid that is in the region below the solubility curve (*i.e.,* under the blue dashed line) is considered supersaturated, and in the unstable region is where spontaneous nucleation can occur.[1, 4] However, spontaneous nucleation is often restricted by confining a system to the metastable region (the area between the two lines), so as to avoid excessive small particle formation.[3]

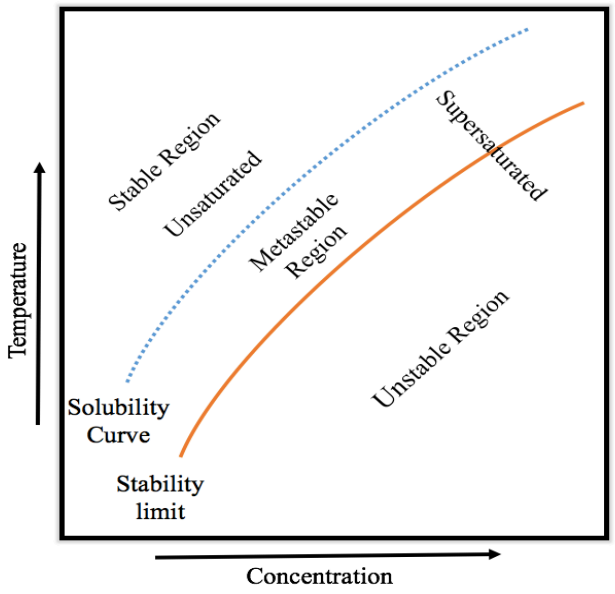

Figure 1. A simplified diagram illustrates the three regions of the solubility curve (adapted from reference 3).

1.3 Calcium Oxalate Crystallization

Calcium oxalate (CaOx) is a mineral that exists in nature as a solid. The term mineral refers to any solid-inorganic compound that occurs naturally, with a well-defined crystal structure and chemical formula. CaOx also is called a biomineral when living organisms produce it.[16] CaOx is naturally found in three different forms. The monohydrate ($CaC_2O_4 \cdot H_2O$, COM) form is called whewellite, and it is named after William Whewell.[17] Whewell was a well-known figure in the 19th century who studied many subjects including geology, mineralogy, and mechanics. COM is considered the most common form of CaOx.[16, 18] The dihydrate ($CaC_2O_4 \cdot 2H_2O$, COD) crystal is called weddellite. This term originated from the Weddell Sea that was named after James Weddell, an Antarctica explorer.[19] COD is less frequently found compared to COM. The trihydrate form ($CaC_2O_4 \cdot 3H_2O$, COT) known as caoxite, is a less common morphology of CaOx, and it is found mainly in pathological stones.[16] CaOx crystallization has received a significant amount of attention because its presence in certain biological, industrial and geological systems can trigger undesirable effects that are difficult and costly to treat.[16, 18]

For example, scale deposits of CaOx in mechanical equipment are the most intractable scale constituent to remove.[20] Scale formation of CaOx (commonly COD on the calandria tubes of sugar mill evaporators) occurs either because sugar cane contains oxalic acid or some substances of the sugar juice decompose into oxalic acid.[21] The Ca^{2+} is absorbed from the soil by the sugar cane plants.[22] CaOx precipitation reduces heat transfer, leading to significant losses of energy, with the related risk of overheating.[21] In addition, the internal diameter of pipes decreases as the scale thickness within these pipes

increases. Therefore, more pump pressure is needed to push fluids through the pipes.[20, 21] Mechanical equipment is maintained in optimal condition by removing the deposits using cleaning chemicals. This treatment is costly and produces toxic effluents.[21]

Details about the formation of CaOx in the geological domain is controversial. Patinas, which are thin layers containing a mixture of calcium oxalate, microorganisms, and other compounds (*e.g.,* calcite, hematite, siliceous sand, and hydroxyapatite) form on historical buildings, marble, artifacts, and monuments.[23] The presence of CaOx patinas is not limited to a particular historical period. Since the 19th century, scientists seeking to determine the causes of biodeterioration have obtained a lot of information about the origins of patinas. An investigation of a sample taken from the Leaning Tower of Pisa suggests that the metabolic activity of microorganisms, like fungus, leads to the formation of calcium oxalate film.[24, 25] The chemical aspect of this hypothesis is that the reaction between calcium and oxalic acid forms CaOx.[24] According to a report at the end of 19th century, Mediterranean patinas of calcium oxalate were the first and most prominently observed on the Parthenon.[26] The deposits of calcium oxalate film on some ancient art monuments' surfaces affected their stone substrates and external appearances. The accumulation of any type of patinas on a monument causes harm to the stone substrates by producing an irreparable loss of their aesthetic appearance and physical strength.[27] However, in some cases, the accumulation of certain species of bacteria and fungus can be beneficial to the monuments. These species are inherently capable of providing protective resins and can be used as energy sources.[27]

Crystallization of CaOx also occurs spontaneously in living organisms. A popular example is the formation of CaOx in human urinary tracts. For instance, an investigation

(in 1901) of thousands of Egyptian mummies found urinary stones in only a few mummies.[28, 29, 30] The archeologist E. Smith found the oldest renal stone (5000 years).[29, 30] In 1905, Shattock described these renal stones.[30] The investigation of Egyptian mummies only reported four cases of urinary tracts which contained urinary stones, and this reflects how less common the stone was in the ancient history.[28, 31] Now, kidney stones are a prevalent clinical issue associated with many factors.

First, understanding how stones form inside the body and what promotes stone formation is a key to determining a strategy that mitigates stone formation. Nephrolithiasis, ureterolithiasis, and cystolithiasis are terms used for stone formation in kidneys, ureters, and bladders respectively. Urolithiasis refers to any stone's formation within urinary system. Urine is composed of macromolecules (mainly mucoproteins and glycosaminoglycans) and dissociated organic compounds, *e.g.,* citrate, oxalate. Urine also contains uric acid and inorganic ions, such as Ca^{2+}, Mg^{2+}, Na^{+}, PO_4^{3-}, HCO_3^{-} and Cl^{-}.[32] The most common urinary stones contain CaOx, calcium carbonate ($CaCO_3$), calcium phosphate, cysteine, uric acid, and struvite. CaOx represents 70-80% of kidney stones.[18] The high concentration of free ions in urine is a critical factor that promotes the formation of the crystals.[32]

For instance, having high concentrations of Ca^{2+} and $C_2O_4^{2-}$ can trigger the formation of COM and COD. A study by Wesson and Ward about pathological biomineralization of COM and COD reports that (1) COM is the prevalent type of kidney stones and (2) surrounding urinary macromolecules adsorb onto primarily COM crystal surfaces during bioformation, thereby promoting the adhesion of these crystals to renal cells at the papillary tip.[18] This adhesion aids aggregation of CaOx to form stable crystal

aggregates.[33, 34] COD is a less common component in kidney stones, and usually found as micron-sized (> 10 micron) single crystals in voided urine. The occurrence of COD single crystals suggests that COD is incapable of forming stable aggregates and firmly adhering to renal epithelial cells. Therefore, the formation of COD is considered a protective agent against kidney stones.[18] Another significant factor that controls the formation of crystals is the presence of inhibitors. The existence of certain compounds in urine, *e.g.,* citrate, can influence the growth of COM crystals by binding to crystal surfaces.[35] Using poly acrylic acid, poly glutamic acid, and poly aspartic acid as inhibitors *in vitro* prevents the formation of COM growth and leads to the creation of COD crystals.[36] The presence of inhibitors and the concentrations of Ca^{2+} and $C_2O_4^{2-}$ in urine are significantly important aspects that explain why large crystals form in some patients and not in others.[16, 18, 36]

In addition, geographic region, ethnic distribution, and socio-economic level play a crucial role in urolithiasis.[31] In the western hemisphere, the percentage of stone formation in adults seems to be higher than in the eastern region. For example, the percentage of people with urinary stones in the Europe, Canada, and the USA is 5-9%, 12%, and 13-15%, respectively.[37] However, Saudi Arabia has the highest proportion at 20.1%.[38] Citizens in countries with hot or warm weather experience higher incidences of urinary stones possibly because of limited fluid intake and low urinary output. Therefore, dehydration is believed to be a major agent in stone diseases. For instance, a study reported that the rates of urinary stone occurrence increase in the Fall and Summer as the temperatures increase.[39] Furthermore, race and gender are also considered important factors. The incidents of urinary stones in Brazil and USA was 4:1 when comparing

Caucasians to Blacks. Also, an increasing of urinary stone formation in Black Americans who adopted the dietary habits of Caucasians.[40] Males have a higher percentage than female, in the United States, 6% of women and of 15% of men suffer from kidney stones.[41] Changes in socio-economic level can cause changes in dietary habits which affect the chemical composition and location of renal stones inside the body.[31]

Some types of kidney stones are more common in some regions than others. For instance, reno-ureteral stones (that mainly consist of CaOx and calcium phosphate) are widespread in developed countries while bladder stones, which are composed of ammonium urate and CaOx are common in Asia.[42] Many other significant factors are also related to stone formation, such as genes, hypocitraturia, and hypercalciuria. The last two are related to dietary habits. The formation of stones can be genetic. For example, a study of 31 children from Kuwait reports 60-90% of renal stones were CaOx with 58% of families who have a history of renal stones.[43] Hypocitraturia is caused by an abnormally low concentration of citrate in urine. A study diagnosed 86 patients using different characteristics and parameters to see the effects of these risk factors, stated that hypocitraturia was the most common factor in 60% of the patients followed by hypercalciuria and low volume of urine.[44]

Extensive efforts have been made to understand CaOx formation details, such as chemical structure, nucleation, and growth kinetics, the external appearance and internal structure.[16, 18, 20, 32, 45, 46, 47, 48] However, an effective solution to prevent and treat this health concern does not exist yet.[16, 18] It is challenging to study the accumulation of CaOx *in vivo* because of the difficulty, if not the impossibility of controlling the parameters in a biological system. Instead it is easier to study simplified systems and extrapolate the

knowledge to more complicated systems.[20, 32, 46] In order to obtain fundamental insight into CaOx crystallization, methods for CaOx crystallization study have been developed.[45, 49, 50, 51]

1.4 Methodologies for CaOx crystallization

Several methods have been used to study the CaOx crystallization process.[46, 51, 52] One of them is the bulk solution method (also called the batch method).[51] This method is based on mixing supersaturated solutions in a vessel to form crystals, filtering the solution, and drying the crystals.[1, 8] In the batch crystallization method, produced crystals are collected at the end of this process.[1, 2] The main issue in this approach is inconsistent results with regard to the number and size of produced crystals.[1, 2, 8, 51]

The aforementioned problem of inconsistency using the batch method has motivated others to cultivate techniques that can help minimize these difficulties since, in some cases, the quality of the crystals is a very significant aspect, *e.g.,* in pharmaceutical crystallizations.[8] Indeed, reproducibility is needed to obtain quantitative determination of nucleation and growth rates.[51] Moreover, crystallization of certain chemical species cannot be achieved in large-scale batch systems because of the disadvantages of this method: high amounts of substance consumption, turbulent conditions, poor manipulation of small fluid volumes, precise control of the temperature and concentration gradients, time consumed and so on.[53] These methodological problems have led to more suitable methods that provide better reproducibility.[51]

1.5 Microfluidic systems; historical background

Microfluidics has been used in a variety of disciplines, such as chemistry, drug discovery, biology, physics, and biomedical studies.[54, 55] The development of micro-scale

systems to provide optimal conditions for various applications started in the 1970s. The first attempt to miniaturize gas chromatography (GC) systems was done by Terry *et al.* at Standord University.[56] Further developments were made to analyze aqueous solutions that contained a complex mixture of substances, such as protein and DNA.[57] The development of microfluidic systems for aqueous solutions studied by capillary electrophoresis (CE) and liquid chromatography (LC) was mainly initiated in four laboratories: the Manz, Ramsey, Harrison, and Mathies laboratories. The techniques that were used to make these systems involved etching silicon and glass and using photolithography.[57]

1.6 Fabrication of microfluidic devices

In 2000, a simple technique called soft lithography was used to fabricate microfluidic devices.[57] Soft lithography is a replica molding process that uses an elastomer, typically polydimethylsiloxane (PDMS).[57, 58] In 2005, the most frequent techniques that were used to fabricate microfluidic devices included photolithography, wet etching, conventional machining, hot embossing, reactive ion etching, injection molding, laser ablation, and soft lithography. Determining a suitable method to fabricate a device depends on several factors, such as cost, available equipment, capabilities of fabrication (required size and profile), and speed. Soft lithography has emerged as the most common technique because it is relatively inexpensive, fast, and suitable for a range of on-chip applications.[58]

To produce a PDMS device, using soft lithography, a master structure is needed. The manufacturing of the master structure using UV photolithography can be complicated for researchers who have little or no experience in microfabrication. Also,

using the laser fabrication method or UV photolithography method to create a 3D device, which consist of either single or multiple channels is complicated. Saggiomo and Velders recently demonstrated that a 3D printer can be used to print a master structure for soft lithography.[59] Another study reported the fabrication of a whole 3D device directly without molding.[60] However, this study relied on mixing a colored photoresist with PDMS, which produced non-transparent devices. Using PDMS is preferred over other kinds of 3D printing plastic due its remarkable features. One such feature is its transparency that allows optical access. Another is its gas permeability, which is an important feature, especially in research dealing with cells and bacteria. Gas permeability keeps bacteria and cells alive for extended periods of time. Another feature is its elasticity, which enables the creation of microvalves and pumps in the device.[59]

1.7 Microfluidic systems for crystallization study

Microfluidic systems enable the manipulation of fluids at the sub-millimeter scale.[52, 57, 61] Compared to other techniques, these systems provide a unique environment to study crystallization because of their unique properties that include their superior heat and mass transport control, the small amounts of samples needed, and the ability to preform real-time monitoring. Flow in all microfluidic systems is laminar. In general, the flow can be either laminar (smooth flow) or turbulent (disordered flow), and the type of the flow depends on the Reynolds number $\left(Re = \frac{Inertial\ forces}{viscous\ forces}\right)$.[53] In the Reynolds number regime of 2300 or less, flow is laminar.[58] In laminar flow systems, mixing only occurs by diffusion.[53]

1.8 Types of microfluidic devices

Currently, there are several types of microfluidic devices: droplet-based, non-droplet-based, valve-based platforms, digital microfluidics, and well-based approaches.[53] However, the two most common systems are droplet-based and non-droplet-based (Figure 2). Studying crystallization using continuous flow platforms is particularly appealing for crystal synthesis because of their relative simplicity. Crystal adhesion to the channel wall is routinely a problematic issue because it leads to blocking of the channel and clogging of the device.[51, 52] Therefore, droplet-based systems are often used for crystallization. In these systems, a droplet is generated by flowing reagents towards a junction that contains immiscible fluids. The immiscible fluids work as carrier fluids that isolate the reagents and inhibit the interaction of the crystals from each other and the channel wall.[51] It is necessary to carefully define reagents and their concentration to regulate the surface chemistry so as to enable the formation of a droplet and ensure that the droplet remains isolated under different experimental conditions, *e.g.,* temperature. In addition to the above considerations, some issues, such as separating and recycling the immiscible phase still exist.[53]

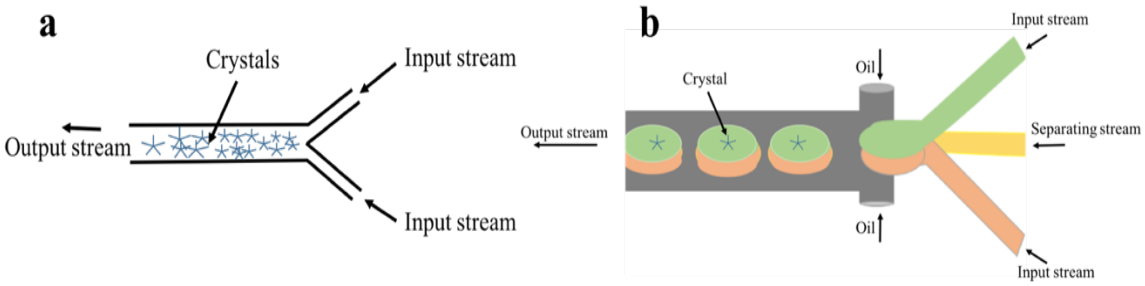

Figure 2. Schematic of (a) a non-droplet-based and (b) a droplet-based microfluidic device (adapted from reference 53).

1.9 Some relevant crystallization studies using microfluidic devices

A calcium carbonate ($CaCO_3$) crystallization study by Yashina *et al.* compared results obtained by three different crystallization methods: the bulk method, droplet-based and non-droplet-based microfluidic devices. They examined $CaCO_3$ crystallization using an equal amount of equimolar calcium chloride and sodium carbonate aqueous solutions. Their conclusion was that using the droplet-based systems provides the best control of the nucleation and growth process resulting in narrow size distributions. In addition to providing relatively narrow distributions, the presence of impurities was limited in droplet based devices. In contrast, in the continuous flow systems, a relatively large range of crystal sizes was obtained, and this is because of the different residence time of each crystal within the device. Therefore, it is difficult to control crystal growth in continuous flow systems. In the bulk method, in addition to obtaining a large range of size distribution and irreproducibility, the existence of impurities and the container walls can cause nucleation.[51]

Despite the pitfalls of using a continuous flow system, it is still the most preferred platform among the different microfluidic systems. For example, a recent study by Sultana *et al* used continuous flow microfluidic systems to examine pharmaceutically active compounds.[52] The crystallization of small organic compounds is hard to accomplish in continuous flow microfluidic systems. This is because of problems such as wall interactions, unmanageable nucleation and growth rate, and precipitation of crystals that can block the channel and clog the device. The study by Sultana *et al* established a unique design of a continuous flow system that solves these issues. Their design separated the nucleation process from the crystal growth, and regulated the secondary

nucleation and agglomeration. Modifying the channel surface enabled them to control the interaction of the crystals with the channels, and accumulations of crystals was controlled by using particular concentrations of the reagents. Their work demonstrates that with a suitable design of a continuous flow platform, the problematic issues of this platform can be mitigated.

1.10 Research objective

The overall goal of this research was to fabricate a microfluidic device that provides a means of studying the influence of various parameters (*e.g.,* Ca^{2+} and Ox^{2-} concentration and additives) on the CaOx crystallization process in a reproducible manner. The choice of a continuous flow system is to limit the complexity of the system by not requiring the formation of droplets. A continuous flow system would inherently need a relatively lower (compared to conventional bulk crystallization methods) amount of material for an analysis, thereby making it an attractive solution for instances where particular materials are costly or hard to acquire. Thus, in this work, a specific objective is to demonstrate that a particular microfluidic design enables one to obtain the same or similar results to those obtained in conventional labware. To achieve this objective requires

(1) the development of an appropriate design to reduce crystal adhesion to the channel walls

(2) a protocol for device operation

(3) a set of experiments that allow a comparison between results obtained with the device to results in previously published reports.

1.11 Thesis outline

This dissertation will describe a microfluidic device design that enables control of where crystallization occurs within a device, and it will demonstrate that this control can be used to eliminate or reduce crystal sticking to the channel walls. In addition, the protocol for generating this device will be described. Finally, (1) the formation of calcium oxalate crystals using the aforementioned device and (2) the influence of certain additives of the CaOx process will also be detailed. This study of CaOx crystallization utilized various microscopies, and this use of common methods facilitates comparison of the results obtained here with previously published data. Experimental procedures and the instrumental methods used in this study will be introduced in Chapter 2. Results, and a discussion of these results, will be presented in Chapter 3. Chapter 4 summarizes the main conclusions of this study and outlines future directions.

2. Experimental procedures

2.1 Materials

2-Propanol (99.5%), acetone (99.5%), ethanol (99.5%), potassium oxalate monohydrate ($K_2C_2O_4 \bullet H_2O$, 99.5-101.0%), calcium chloride ($CaCl_2$, ≥93%), and sodium polyacrylate (NaPA, Mw ~5100) were all purchased from Sigma Aldrich. Acryloxypropyl trimethoxysilane (95%) and tridecafluoro-1,1,2,2- tetrahydroctyl dimethylchlorosilane were obtained from Gelest. Trisodium citrate (NaCit) was acquired from Fisher Scientific. Dipentaerythritol pentaacrylate (Sartomer SR 399) and tris (2-hydroxy ethyl) isocyanurate triacrylate (Sartomer SR 368) were the oligomers used to make the resin (*i.e.,* the photoresist). The photoinitiator in this resin was ethyl (2,4,6-trimethylbenzoyl) phenylphosphinate (Lucirin TPO-L, BASF). A PDMS elastomeric kit (Sylgard, Dow Chemical) was used to make the devices. The tubing for all devices was polytetrafluoroethylene (0.022"ID x 0.042"OD, Cole Parmer). A silicon (100) wafer (~25 mm^2) was purchased from Ted Pella (Type P/100). IR windows, zinc selenide (ZnSe) and barium fluoride (BaF_2), were obtained from International Crystal Laboratories.

2.2 Methods

2.2.1 Acrylate and fluorocarbon coating of glass slides

In this study, functionalized glass slides were created using common functionalization processes. Firstly, microscope slides were washed (~30 sec) in 2-propanol, acetone, and then distilled water. Slide racks were used to hold the slides that were then dried in an oven (~1 hour, 100°C). Next, an oxygen-plasma cleaner (Harrick Plasma, PDC-32G) was used (2-3 min, ~600 m Torr O_2) to obtain hydrophilic surfaces. Immediately after this plasma cleaning, the slides were soaked in a solution of 93 vol%

ethanol, 5 vol% deionized water, and 2 vol% 3-acryloxypropyl trimethoxysilane 95% for ~15 hours. During this time, the solutions were stirred. Next, the slides were immersed in ethanol (~1 hour). After removing them from the ethanol, the slides were dried in an oven (~1 hour, 100°C).

To coat slides with a fluorocarbon, several slides were placed in a desiccator which had a watch glass containing some drops of tridecafluoro-1,1,2,2- tetrahydroctyl dimethylchlorosilane (Figure 3). After evacuating the desiccator, the slides were left in this desiccator (~1 hour) to enable vapor deposition of the fluorocarbon on the slides.

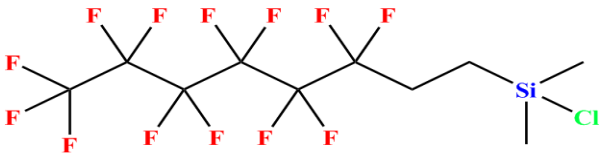

Figure 3. The chemical structure of tridecafluoro-1,1,2,2- tetrahydroctyl dimethylchlorosilane.

2.2.2 Photoresist and PDMS preparation

SR 399 (54 wt %), SR 368 (43 wt %), and Lucirin TPO-L (3 wt %) were mixed to make the photoresist for the acrylated master microstructure (Figure 4). The photoresist was mixed (~18 hours) in a small container to obtain a homogenous mixture. Figure 4d illustrates the polymerization of the acrylate monomer under the UV. To make the PDMS pre-polymer, a 1:11 wt% ratio of the curing agent-to-base from PDMS was stirred and degassed.

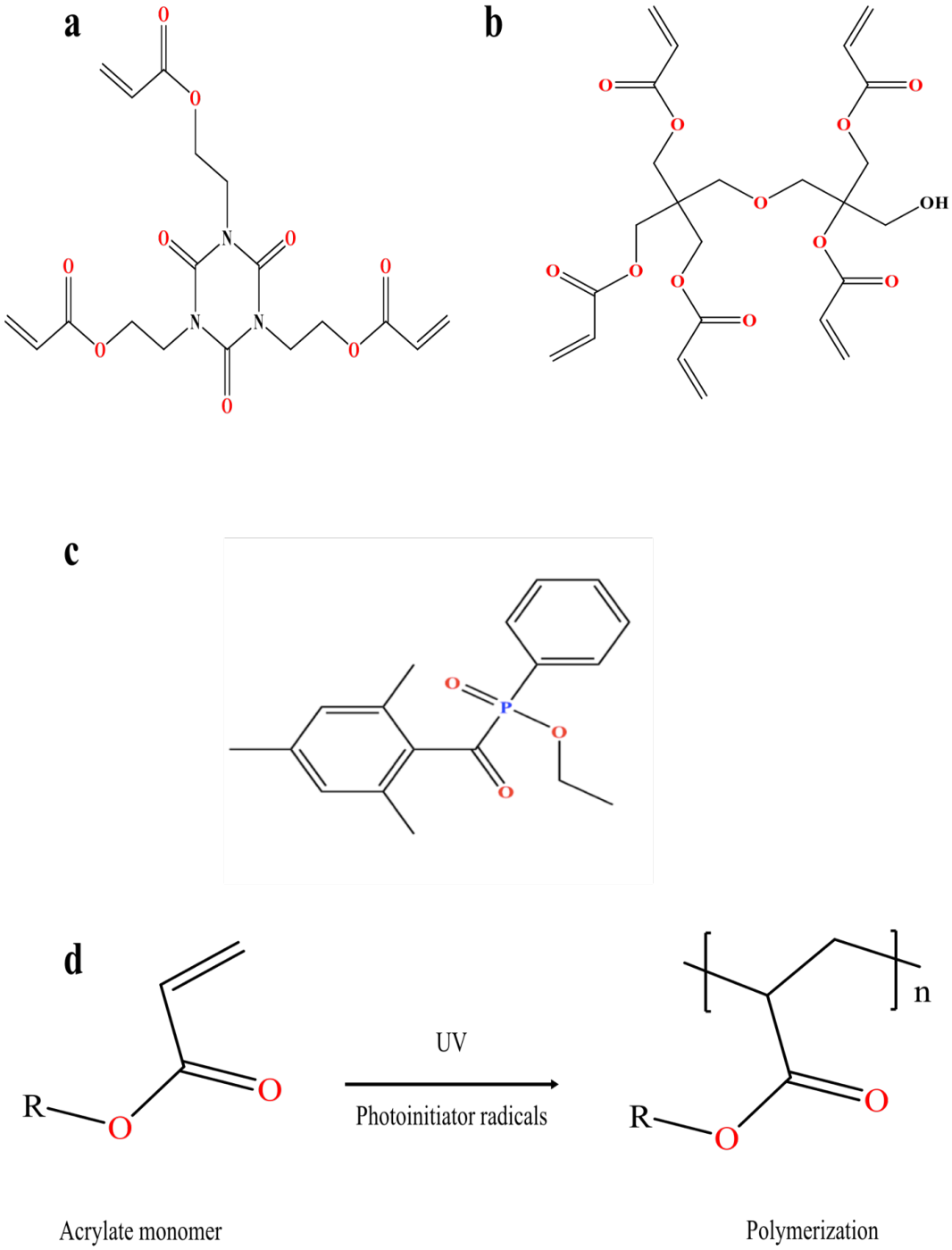

Figure 4. The chemical structures of (a) SR 368, (b) SR 399, (c) Lucirin TPO-L, and (d) the polymerization of acrylate monomers.

2.3 Device design

Supersaturation is necessary to produce spontaneous crystallization. In our device, a supersaturation solution is created by Ca^{2+} and Ox^{2-} (the entities of the two side streams originating from $K_2C_2O_4 \cdot H_2O$ and $CaCl_2$) diffusing into the middle stream. To induce crystallization, the supersaturation ratio, S, of Ca^{2+} and Ox^{2-} must be more than one (*i.e.,* $S > 1$). The supersaturation ratio is defined as:

$$S = ([Ca^{2+}][Ox^{2-}]/ Ksp)^{1/2} \quad (1)$$

The concentrations of Ca^{2+} and Ox^{2-} in the middle stream have to exceed the solubility constant (Ksp) of CaOx crystals ($\sim 2 \times 10^{-9}$) for precipitation to begin. Within the main channel, various regions will have different ratios of Ox^{2-} and Ca^{2+}. The region near the Ox^{2-} stream is richer in Ox^{2-} than it is in Ca^{2+}. Similarly, the region near the Ca^{2+} stream is richer in Ca^{2+} than it is in Ox^{2-}. Therefore, because the supersaturation ratio involves the product of $[Ca^{2+}]$ and $[Ox^{2-}]$, it is inevitable that there will be regions within the main channel with the same supersaturation ratio but with different local concentrations of Ca^{2+} and Ox^{2-}. This is an important fact to bear in mind when examining the crystallization process in this device design (Figure 5).

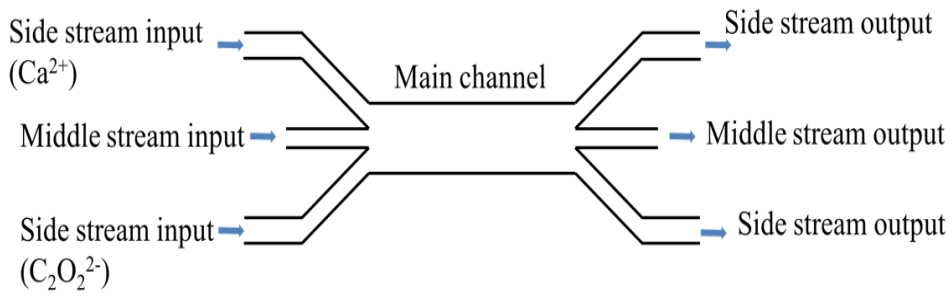

Figure 5. A schematic of the design containing three inputs and three outputs.

2.4 Microfluidic fabrication

2.4.1 UV photolithography and soft lithography

Both UV photolithography and soft lithography are routinely used in microfluidic fabrication. To fabricate microfluidic devices using the soft lithography method, an acrylate master microstructure was needed. To make the acrylated master structure, several layers of tape were put on both sides of a fluorocarbon-functionalized slide. These layers of tape worked as spacers to achieve the desired film height. Then, a few drops (3-5) of photoresist were put on the same slide (Figure 6a). After placing an acrylated slide on top of the fluorocarbon-functionalized slide, a transparent mask (CAD) with the desired design was placed on the acrylated slide. Next, the entire assembly was exposed to a UV light (Black-Ray B-100A, UVP) for ~3 min (Figure 6b). After exposure, the two slides were carefully separated, and the unexposed resin was washed away (by acetone) from the acrylated slide to obtain the master structure. For this washing process, the master structure was immersed consecutively into two acetone baths (1 min each). The obtained master structure was then heated (~4 hours, 75°C) to assist the evaporation of any remaining photoresist. Any remaining photoresist can react with PDMS, and this reaction inhibits PDMS curing. As a result, the obtained PDMS mold would have "sticky" channels. All molds were heated in an oven (100°C, 2-3 hours) after being made to ensure optimal cross-linking.

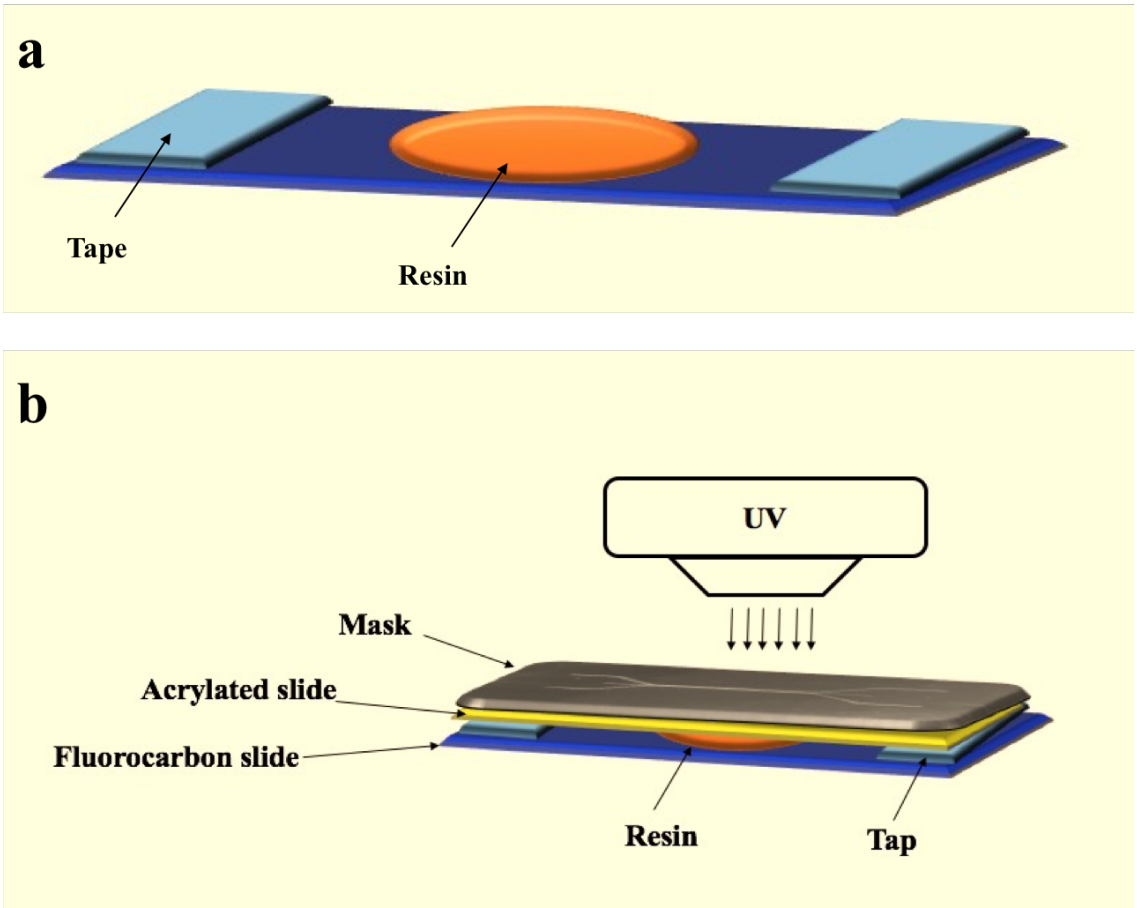

Figure 6. Illustrations of (a) a fluorocarbon-functionalized slide with the tape pieces and resin and (b) the photolithography process to obtain a master structure.

The obtained master structure (Figure 7a) was functionalized using the same process that was used to functionalize glass slides (described in section 2.2.1). The purpose of applying a fluorocarbon-based coating is to facilitate the separation of the slide and master structure from the cured PDMS. To mold the master structure, the slide containing the master was placed on a piece of aluminum foil. This foil was folded to acquire a shape like an open box (Figure 7b). The PDMS pre-polymer mixture was poured on the master (and therefore also on the slide), and the entire assembly was heated (~5 hours, 75°C) to cross-link the PDMS. Afterward, the PDMS mold was separated from the slide, the mold's edges were trimmed, and access holes (three inputs and three

outputs) were bored (Harris Unicore, 1.20 mm) into the mold. Then, the PDMS mold was attached to a flat portion of cured PDMS. To make this flat piece of PDMS, a procedure similar to the one used to make the mold of the master structure was followed. However, instead of placing a slide containing the master on a portion of aluminum foil, a fluorocarbon-functionalized slide was placed on the aluminum foil. These two PDMS pieces (the mold and flat portion) were oxygen plasma-cleaned (~30 sec, ~600 mTorr O_2) and immediately placed in contact with one another. Next, these attached pieces were heated (~5 min), and tubes were placed into the access holes (Figure 7c). The main channel of the device is estimated to be ~350 μm high × 15000 μm long × 1000 μm wide. The cross section dimensions (350 × 1000 μm) were obtained by cutting a device and determining the main channel cross section based on optical images (see Figure 30b).

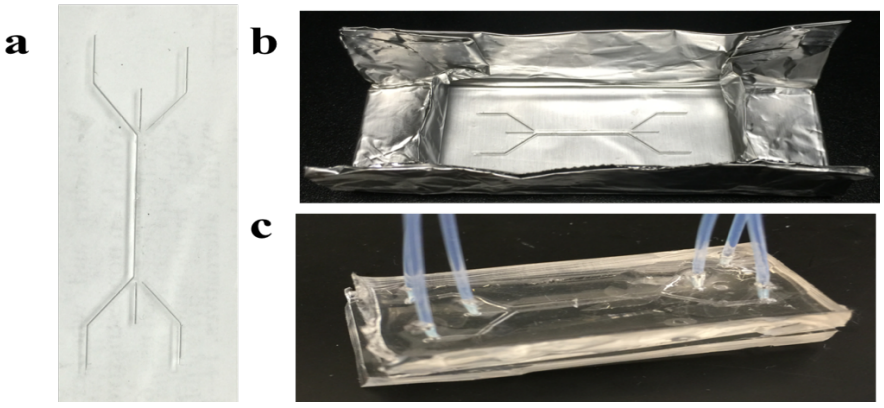

Figure 7. Optical images of (a) a master structure, (b) the master structure on a microscope slide in the aluminum foil box, and (c) a microfluidic device.

2.4.2 3D printing method

In addition to fabrication of the 2D devices (described in section 2.4.1), a process for making 3D devices using a 3D printer was also explored. For this process, the master structure was 3D-printed using a commercial printer (MakerBot Replicator 2X). After

getting a master structure (Figure 8a), the master (which was made out of the ABS polymer (acrylonitrile butadiene styrene)) was placed in a box made of aluminum foil (Figure 8b). The PDMS was poured into the box and cured in the oven (2 hours, ~75°C). Afterward, the block of PDMS was immersed (~12 hours) in acetone. This PDMS block was cleaned using acetone and dried by passing compressed air through the channel. Placing the tubes into the access holes completed the fabrication of the device.

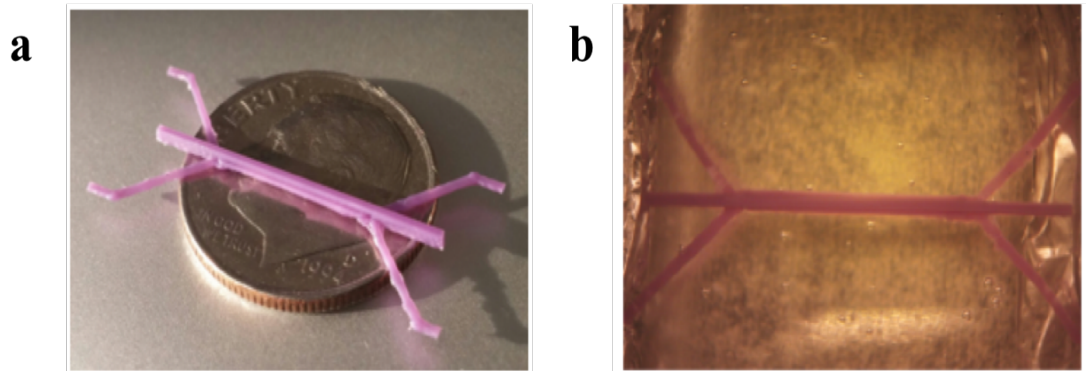

Figure 8. Optical images of (a) a master structure obtained by 3D printing and (b) the replica mold of the 3D printed master structure

2.5 Device operation

It is important, when operating the device, to prevent the formation of bubbles (both inside the device and in the tubes). Bubbles can cause rapid and undesired crystallization that clogs the device and modifies the desired flow characteristic (Figure 9a). A recent study by Wang *et al.* reported a protocol that limits bubble formation in microfluidic devices.[62] They combined a PDMS hydrophilic surface treatment (using ethanol) with vacuum filling to reduce the bubble formation inside microfluidic devices. Their method contained five steps: (1) a microfluidic device was immersed in an ethanol bath (10 min) after being filled with ethanol; (2) the device (in the bath) was placed in a vacuum desiccator (30 min, pressure of ~110-120 kPa); (3) the ethanol bath was switched

to distilled water; (4) the water bath was vacuum treated for 30 min; and then (5) the device was removed from the desiccator, wrapped in foil, and autoclaved. Based on this protocol, we devised a similar method to eliminate bubble formation in our devices.

In our process, the device was placed in an ethanol bath, and then this bath was placed inside an evacuated desiccator (~25 min). Next, three syringes were connected to the three input tubes, and these syringes were placed on three separate pumps (one Kent Scientific Genie Plus and two New Era NE-1000). The three output tubes were placed in three different beakers, with the middle one containing a substrate for collection. Inserting a syringe needle into the middle output tube facilitated the placement of the output tube, which in turn helped the collection process (Figure 9c). Device operation was monitored using a stereomicroscope (StereoZoom 4, Bausch and Lomb). Ethanol was passed (~5 min) through the device to remove any bubbles (using any flow rate).

After this bubble removal and prevention process, the two side streams were switched to dye solutions. The side streams' input syringes were switched from ethanol to dye solutions inside a distilled water bath to prevent bubble formation (Figure 9d). The point of introducing the dye solutions is to help determine the desirable flow rates and the stream widths (Figure 9b). The flow rates (listed below) were carefully selected to limit the diffusion of each stream. In other words, flow rates were selected such that even with dye solutions flowing in the side streams, the middle stream remained relatively clear (Figure 9b). The device was washed to remove the dye solutions by switching to distilled water that was flowed (~5 min) through the channels. The last switch was to the solutions with the crystal components. $K_2C_2O_4 \cdot H_2O$ and $CaCl_2$ were simultaneously pumped into

the device (through the side streams) using 20 µL/min flow rates. These side streams were separated by the middle stream, which had a flow rate of 50 µL/min.

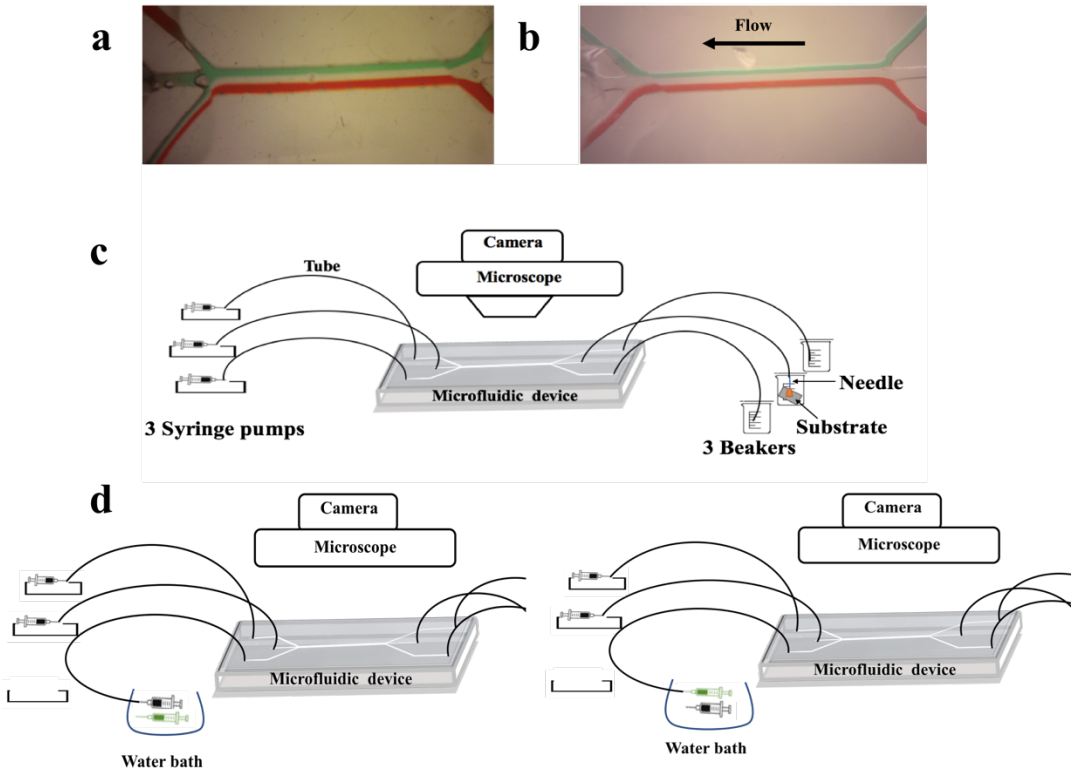

Figure 9. Optical images of (a) bubble formation within the device and (b) the dye solutions used to visualize the flow profile. Illustrations of (c) the experiment set-up and (d) the process of switching syringes inside a water bath.

Different types of substrates were used as collection substrates in this study; these included glass, silicon, quartz, and IR windows (ZnSe and BaF_2). For a particular experiment, one of these substrates was placed in the middle beaker, which was then filled with a supersaturated solution of CaOx to prevent any dissolution of the collected crystals. A particular type of substrate was (*i.e.,* ZnSe, BaF_2 or silicon) chosen to enable crystal characterization using Raman and transmission IR spectroscopy. Crystals were collected for ~30 min, and then the substrate was removed from the beaker and dried at

ambient conditions. After finishing an experiment, any adhered crystals were washed out of the device using solutions of either 2 M HCl or 100 mM NaCit. These cleaning solutions were flushed out by passing deionized water through the device.

2.6 Spectroscopic analysis

To obtain an idea of crystal shapes and types of polymorphs present in our collected samples, the crystals were analyzed with an optical microscope (LV100D, Nikon) using a 10× eyepiece, 20×, and 50× objectives (100–500 magnification range). Further details about the crystal shapes and polymorphs were acquired using a scanning electron microscope (SEM) (LEO1450EP, Zeiss). SEM provides a high magnification (*e.g.,* 40,000×) image by scanning a sample using a focused beam of electrons that interacts with the sample and produces many electrons from the sample. A detector reads the electron intensity from various regions of the sample and creates an image of the sample. To obtain an SEM image, the substrate (with crystals) was first mounted on a carbon conductive tape, and then a gold sputter-coat was applied to the substrate. The same procedure was followed to obtain images of crystals on PDMS.

For determining the chemical composition of crystals, a confocal Raman microscope (Xplora, Horiba) and Fourier transform infrared (FTIR) microscope (LUMOS, Bruker) were used. Different types of substrates were used to collect crystals based on the instrument. Silicon substrates were used for Raman analysis and either BaF_2 or ZnSe was used for FTIR analysis.

The confocal Raman microscope combines an optical microscope and Raman spectrometer, providing unique Raman analysis. This instrument allows a high magnification (up to 1000× with a 100× objective) of an object, and also can analyze

individual layers or particles.[63] This microscope is relatively easy to use. To obtain spectral information using the confocal Raman microscope, the light (photons) interacts with the chemical bonds within a sample, and this interaction changes the vibrations and rotations energy level of the sample.[63, 64] These changes lead to energy transmissions in the sample, and these transmissions produce scattered light that creates a Raman spectrum.[63, 64] The spectrum provides valuable information about chemical composition as well as quantitative and qualitative information about the sample.[63] Proper selection of an objective and an excitation laser power can result in high spatial resolution.[63] In this work, the Raman microscope was calibrated with a silicon slide (520-nm line). Each spectrum was an average of 4 scans collected by using a 5-second acquisition time (the time spent acquiring the signal at each wavelength), a 532-nm excitation laser (6.25 W), a 1200 gr/mm grating, and a 100× objective.

In contrast, an FTIR microscope combines an optical microscope with a FTIR spectrometer. A beam of IR radiation passes through a sample which absorbs some of this radiation and transmits others. Then, a detector gathers the transmitted radiation and displays a spectrum.[65] The spectrum provides information about functional groups that exist in the samples. In this work, crystals were collected on IR windows (BaF_2 or ZnSe) to enable transmission FTIR analysis. Also, FTIR spectra were collected using 4 cm^{-1} resolution with an unpolarized excitation beam and 8× objective. Each spectrum was an average of 512 scans. Wavelength calibration for the FTIR microscope is done by the software for this instrument. The detector in this FTIR microscope is mercury cadmium telluride (MCT).

At certain excitation powers, the radiation used in confocal Raman microscopy can damage samples[63]. However, no visible changes or damage to the crystals were observed in the experiments described in this study. Using a confocal Raman microscope enabled us to focus on small particles making it more preferable than a FTIR microscope. Another reason to prefer Raman microscopy is that this method has a better spatial resolution due to the shorter wavelength that is used in it.[63] The infrared excitation powers used in infrared analysis do not produce any permanent changes or damages to samples.[66] However, FTIR microscopes have low absorbency and restrictions in their spatial resolution which limit their ability to provide information about isolated crystals except when the crystal is larger than 15 μm.[65]

2.7 Experimental approach

The same microfluidic device was used in all experiments, and each experiment was repeated at least three times for reproducibility. Initial experiments used the same concentrations of Ca^{2+} and Ox^{2-} in the two side streams. In these experiments, the input concentrations of Ca^{2+} and Ox^{2} were increased systematically (over the 10 - 80 mM range) to discern the effects of the input concentrations on CaOx crystallization; the same flow rates were used for these experiments. Also, non-equimolar Ca^{2+} and Ox^{2-} input concentrations of 80 and 20 mM, respectively, were used. Then, 20 and 80 mM of Ca^{2+} and Ox^{2-} input concentrations, respectively, were examined. These non-equimolar input concentrations were used to obtain information about their influences on the CaOx formation process. The effects of certain chemicals, such as NaPA, NaCit, and HCl were also studied as described in the introduction as they are known to inhibit CaOx crystallization. These chemical species were introduced as the middle stream.

3. Results and discussion

3.1 Equimolar Ca^{2+} and Ox^{2-} input concentrations

In this chapter, a convention for specifying the input concentrations of Ca^{2+} and Ox^{2-} in the two side streams will be used. In this convention, a $CaCl_2$ and $K_2C_2O_4 \cdot H_2O$ input concentration of 20 mM and 20 mM, respectively, will be represented as (20, 20 mM). Similarly, a $CaCl_2$ and $K_2C_2O_4 \cdot H_2O$ input concentration of 20 mM 80 mM, respectively, will be written as (20, 80 mM).

There are terms used to identify the CaOx crystals based on their shapes.[67, 68, 69] Therefore, the morphology of CaOx crystals that were obtained from all experiments (in different conditions) are displayed in Figures 10 and 11 for clarification. Figure 10 shows COM crystals including twin, X-shaped, dendrite, and agglomerate crystals whereas Figure 11 shows different COD crystals.

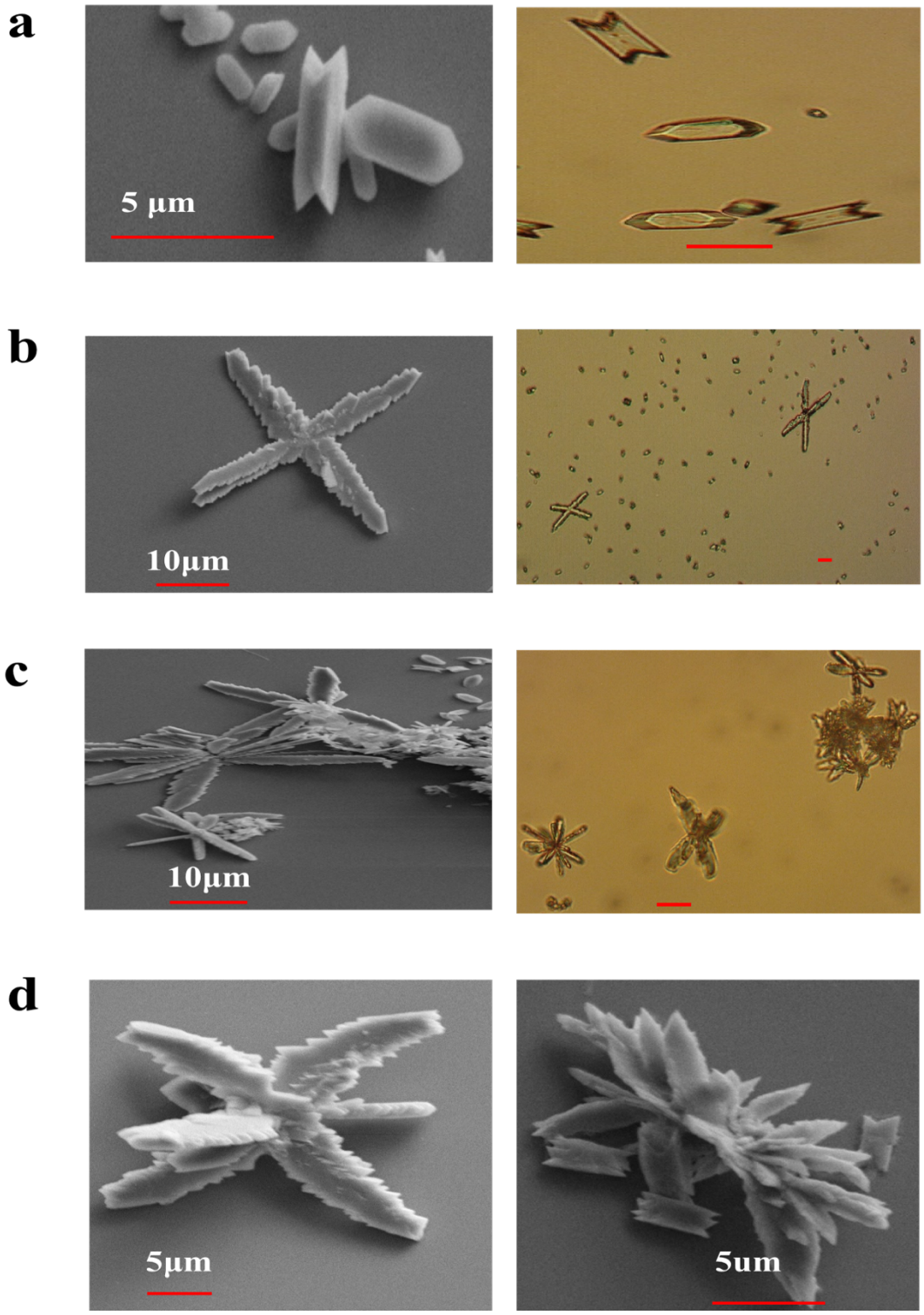

Figure 10. Different COM shapes that were acquired: (a) twin, (b) X-shaped, (c) dendrite, and (d) agglomerate crystals. The scale bars of the optical images are 10 µm.

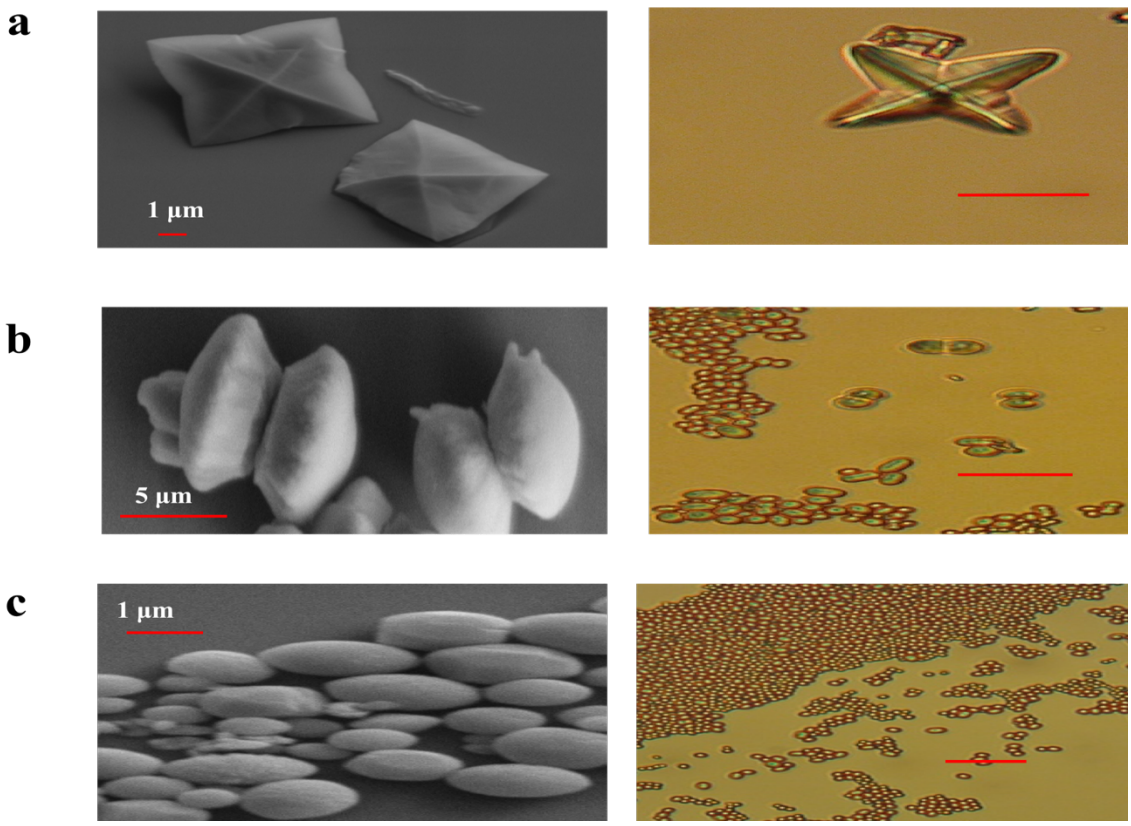

Figure 11. Different COD shapes that were obtained: (a) tetragonal bipyramid, (b) dumbbell, and (c) rounded crystals. The scale bars of the optical images are 10 µm.

Experiments using equimolar input concentrations of Ca^{2+} and Ox^{2-} revealed that a line of crystals formed at the center of the main channel (during the flow of these species through the device) for concentrations of (30, 30 mM) or more. At concentrations of (20, 20 mM) or less, no such line was observed. The line of crystals within the device increased as the concentration increased (Figure 12a). In the (30, 30 mM) experiments the crystal line was thin and light (less than 50 µm) as shown in Figure 12b, and the thickness of the line increased as the input concentrations increased (Figure 12c). For example, (80, 80 mM) experiments produced a thick crystal line (more than 50 µm) at the beginning of the reaction. However, for the (30, 30 mM) experiments, the line produced was light and thin (difficult to see at the beginning of the experiment) (Figure 12b and c).

The thickness and the length of crystal line was directly related to the Ca^{2+} and Ox^{2-} input concentrations. As more Ca^{2+} and Ox^{2-} ions diffuse into the middle stream, more precipitation of these ions occurs causing the formation of the crystal line. The crystal line only formed near the center of the main channel. Therefore, it can be assumed that crystals are forming in regions where the $[Ca^{2+}]$ and $[Ox^{2-}]$ are roughly the same.

What the starting point of the crystallization line represents is debatable. At the very least, the first point of this line is the point where crystals (formed either at or before this point) agglomerate and stick to the main channel wall. The line of crystals adhered to the bottom of the main channel, and this fact was noticed after separating the two molds (*i.e.,* PDMS pieces of a device) to acquire SEM images of the crystal line (Figure 12d). Replacing the bottom PDMS piece of the device allows the device to be reused. Why crystals do not adhere to the top of the main channel is currently unclear.

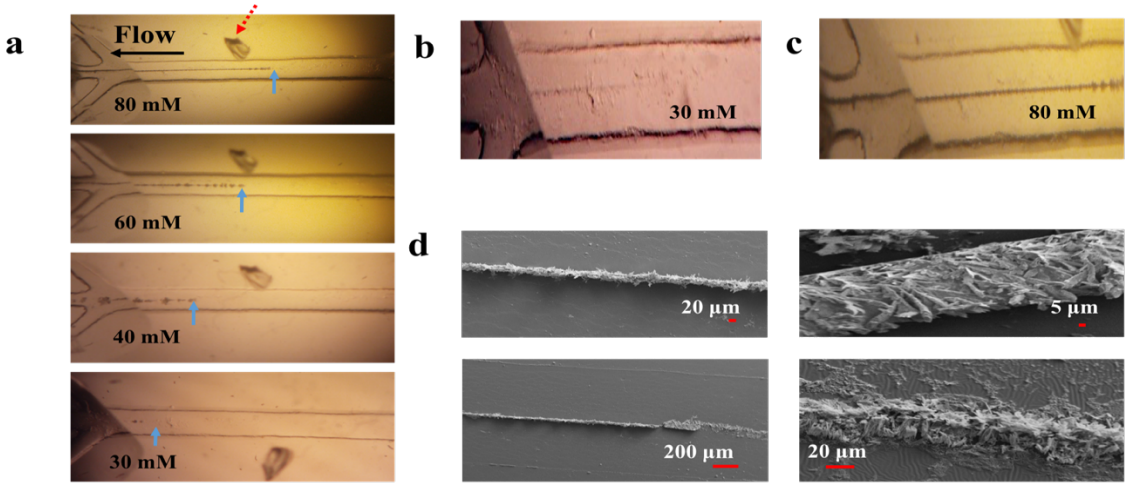

Figure 12. Optical images of (a) the line that formed in devices during CaOx crystallization experiments at four different input concentrations using a magnification of 70×. The red dotted arrow points to a small divot in the PDMS that helps to distinguish the end point. The blue arrows indicate the end point of the line and the black arrow (in the first image) indicates the flow direction in all experiments. Optical images showing the thickness of the crystal line using a 250× magnification of (b) 30, 30 mM and (c) 80, 80 mM experiments. (d) SEM images of the crystal line of an 80, 80 mM experiment.

Even though no line was seen in experiments using (20, 20 mM) and less, small crystals were found on the collection slide (Figure 13a). For the (20, 20 mM) experiments, many small crystals (less than 5 μm) were obtained (Figure 13a). Also, almost all the crystals found were COM twins (Figure 13a). For the (30, 30 mM) and (40, 40 mM) experiments, a range of shapes, sizes, and morphologies of CaOx crystals were found. For these two concentrations, the presence of COD tetragonal bipyramid crystals was observed, and most collected crystals were COM twins with some COD tetragonal bipyramids (Figures 13b and 15). The collection slide of the (40, 40 mM) experiments (Figure 13b) contained more COD tetragonal bipyramids than the collection slide of the (30, 30 mM) experiments (Figure 15). The collected crystals from the (30, 30 mM) experiments were relatively smaller (less than 5 μm) than the crystals that collected from the (40, 40 mM) experiments.

The shape dispersity and crystal size increased as the input concentration increased. For the (60, 60 mM) and (80, 80 mM) experiments, in addition to the existence of crystals that were found in the (40, 40 mM) experiments, X-shaped COM crystals, COM agglomerates, and COM dendrites (crystals having arms) were also present (Figures 13c and 14). Also, the quantity of tetragonal bipyramids increased as the input concentrations increased (Figures 13 and 14). In the (60, 60 mM) and (80, 80 mM) experiments, the single maximum size of the crystals was between 15-25 μm (Figures 13 and 14). The most common morphology observed in all equimolar experiments was COM. It was difficult to obtain further details about the CaOx crystal shapes and sizes because of the significant amount of aggregation of single COM crystals, especially with experiments involving high concentrations of Ca^{2+} and Ox^{2-} (Figures 13 and 14).

Collection time also had an impact on crystal size, and this was observed when the same experiment was repeated using different collection times. For example, in the (30, 30 mM) experiments, the crystals collected during a collection time of ~30 min were smaller than the crystals that collected over a 50 min span (Figure 15). Also, conducting (20, 20 mM) experiments for ~30 min resulted in no crystals on the collection slide. Increasing the collection time to ~90 min yielded many crystals on the collection slide as in Figure 13a.

As previously mentioned, the size and shape of the collected crystals for a particular experiment varied significantly for experiments using (60,60 mM) and (80, 80 mM) input concentrations. On the collection slides for these experiments, different sizes of the same type of crystals were obtained (Figures 13c and 14). There are two possible reasons for this occurrence: the velocity distribution and the position of crystal formation. The velocity distribution in the main channel is not the same. The velocity of the middle stream is higher than the two side streams because of the inherent nature of pressure-driven flow. Therefore, crystals formed near the wall (where the velocity is low) will have a higher residence time, and they will be greater in size. Alternatively, even for crystals formed in areas with the same fluid velocity, it is possible that some crystals are created near the entrance to the middle outlet tubing. These crystals will be smaller than crystals that form further away from this outlet. Based on the fact that the crystal line forms in the center of the middle channel, one can infer that the small crystals (less than 5 μm) obtained in these experiments formed either within the middle outlet tubing or near the exit of the main channel (Figure 13a).

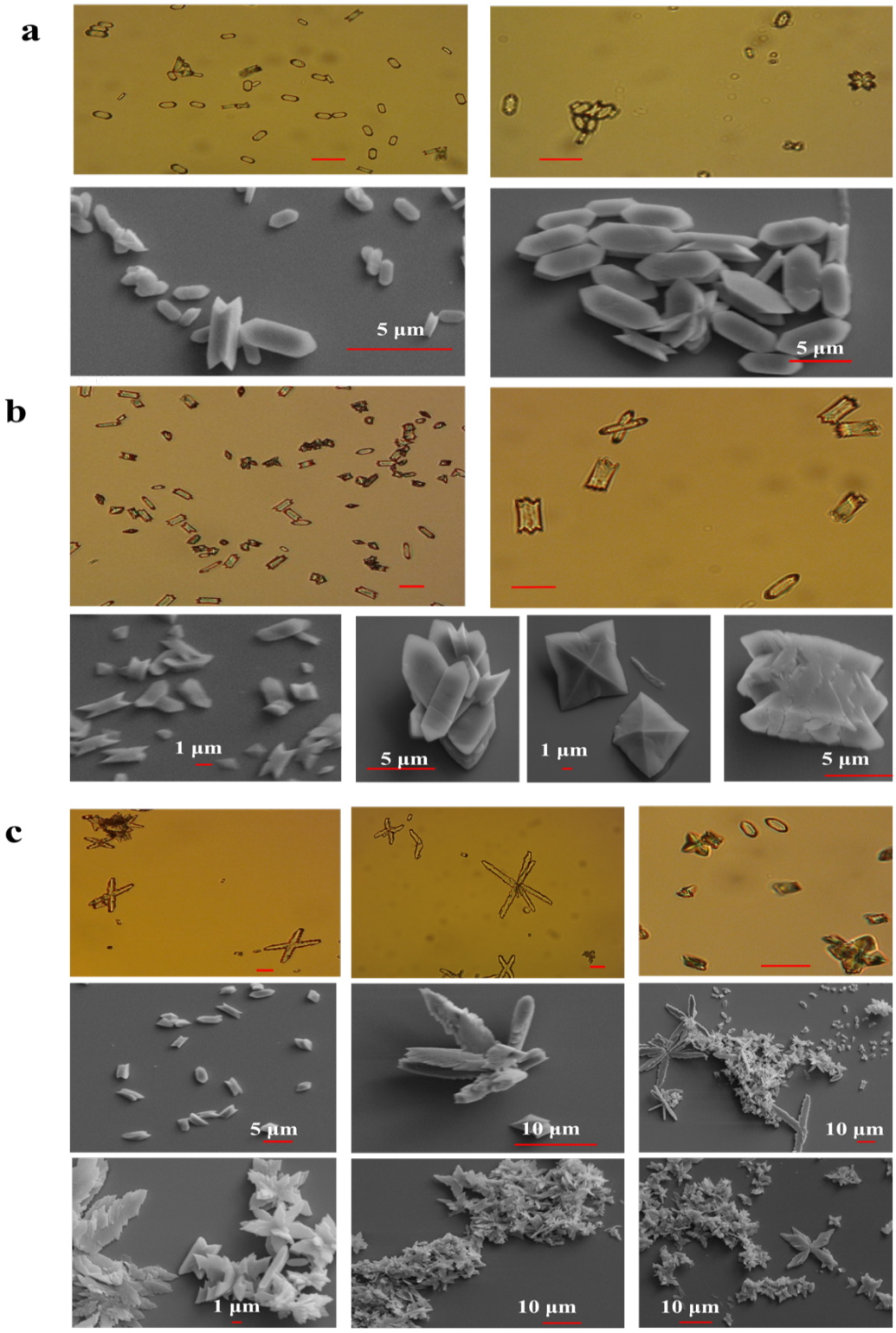

Figure 13. Optical (yellow) and SEM (gray) images of CaOx crystals on the collection substrate for equimolar experiments of (a) 20 mM, (b) 40 mM, (c) and 60 mM. All optical image scale bars are 10 µm.

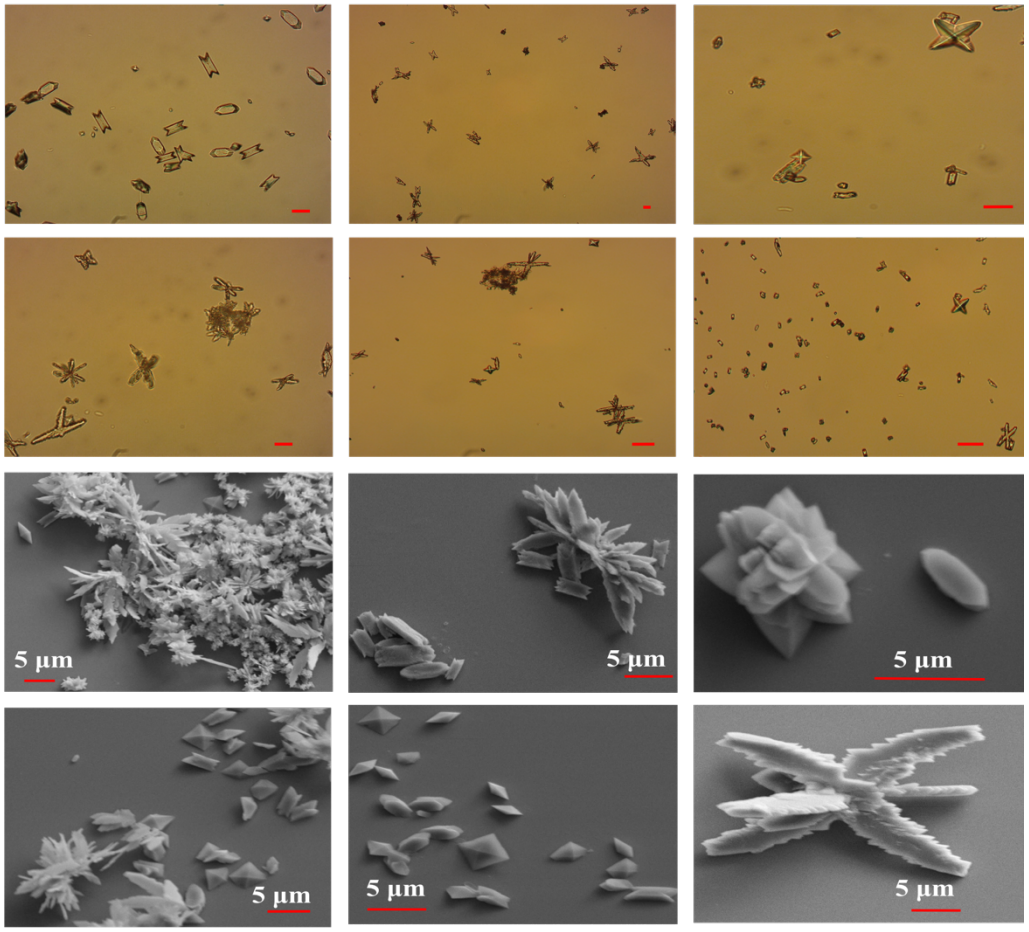

Figure 14. Optical (yellow) and SEM (gray) images of CaOx crystals on the collection substrate of (80, 80 mM) experiments. The scale bars of the optical images are 10 µm.

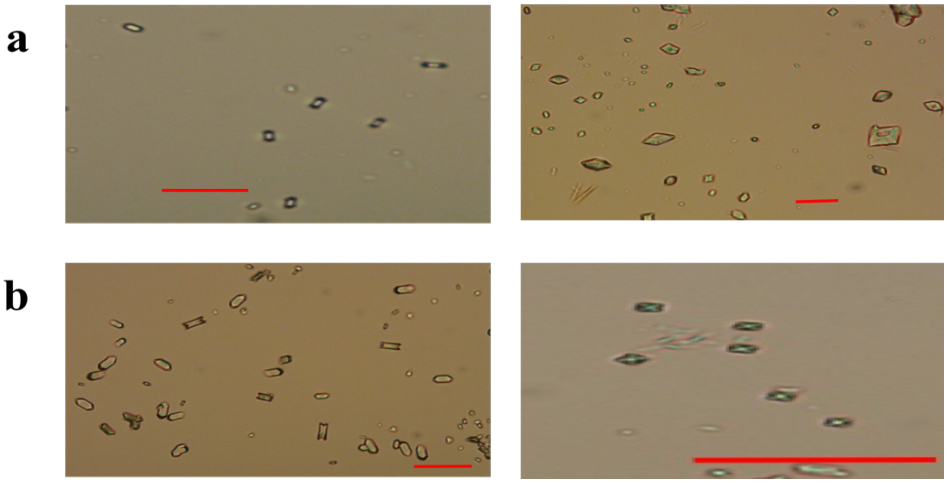

Figure 15. Optical images of crystals that collected at different times for (30, 30 mM) experiments (a) ~30 min and (b) ~50 min. The scale bars of the optical images are 10 µm.

3.2 Non-equimolar Ca^{2+} and Ox^{2-} input concentrations

As described in the previous paragraph, using a range of the same concentrations of Ca^{2+} and Ox^{2-} ions had an impact on the characteristics of CaOx formed. To obtain further details about these effects, non-equimolar Ca^{2+} and Ox^{2-} input concentrations were used. In these experiments, when the Ca^{2+} input concentration was higher than the Ox^{2-} input concentration, the collected crystals had rough surfaces and were more diverse in size (between 1-20 μm). In contrast, when the Ca^{2+} input concentration was lower than the Ox^{2-} input concentration, the crystals were small (less than 5μm), as shown in Figure 16a.

In the (80, 20 mM) experiments, large crystals were acquired (Figure 16b). Since the input concentrations have a direct impact on the supersaturation ratio distribution in the main channel, this distribution was the same in the (20, 80 mM) and (80, 20 mM) experiments before any precipitation. However, when nucleation and growth begin, significant differences in supersaturation distribution can occur. If nucleation and growth does not significantly affect the supersaturation ratio distribution in the main channel, then any crystals in the (20, 80 mM) experiments that form in the main channel center are formed in environments where the concentration of the Ox^{2-} is higher than that of the Ca^{2+}. Similarly, any crystals in the (80, 20 mM) experiments would be created in environments where Ca^{2+} concentration is higher than the Ox^{2-} concentration. Since the crystals collected in the (20, 80 mM) experiments were relatively small, this suggests that decreasing the Ca^{2+} concentration leads to the reduction of the crystal size more efficiently that decreasing the concentration of Ox^{2-}.

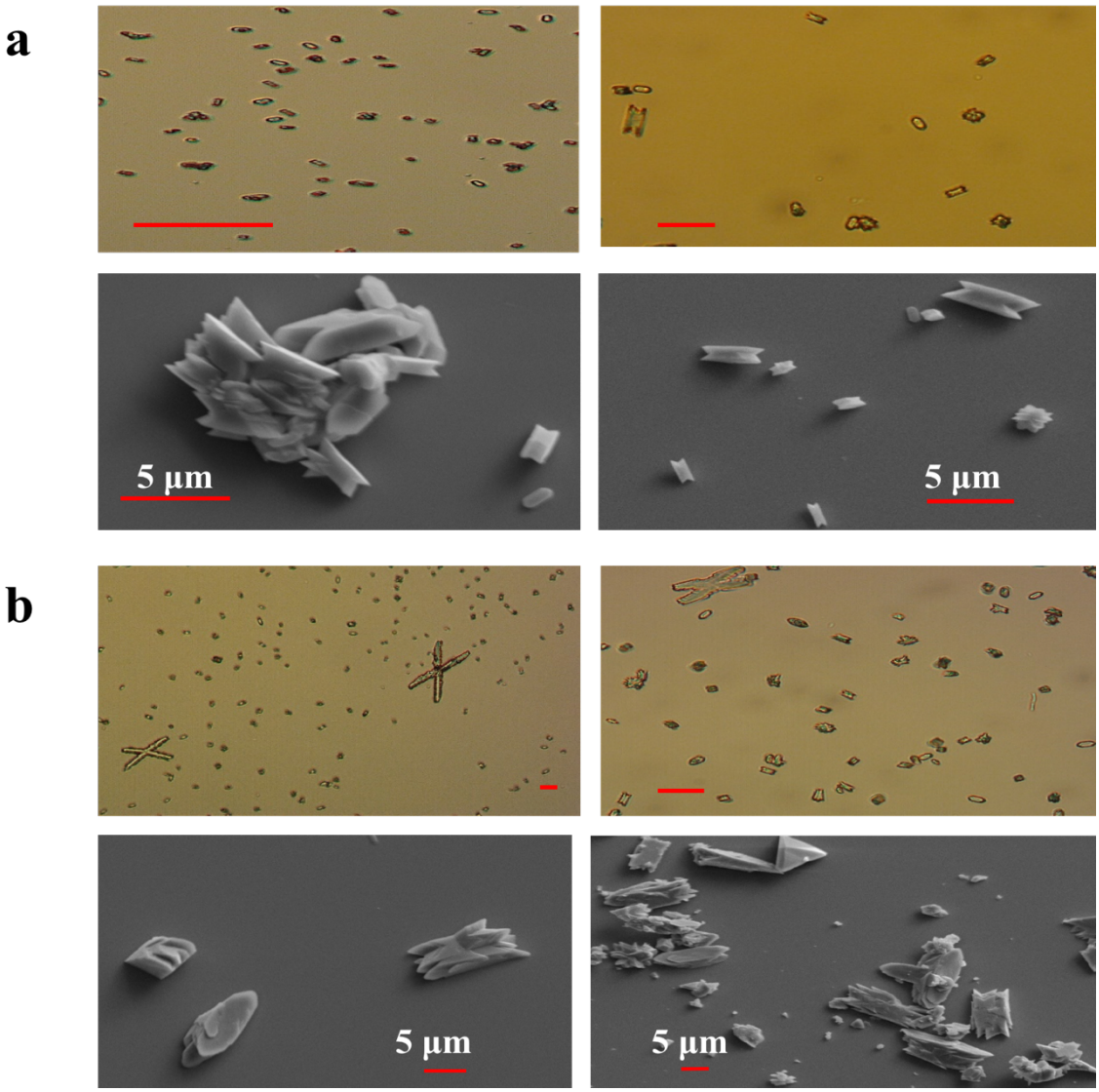

Figure 16. Optical (yellow) and SEM (gray) images of CaOx crystals acquired from (a) (20, 80 mM) and (b) (80, 20 mM) experiments. The scale bars of the optical images are 10 µm.

3.3 Additives

To explore the effects of certain chemical species on CaOx crystallization in our device, these chemical species were introduced as the middle stream. There are numerous studies examining the influence of particular chemical species on the formation of CaOx.[20, 35, 36, 45, 70, 71, 72] NaPA and NaCit have been found to have a significant inhibitory effect on CaOx crystallization.[35, 36, 70, 71, 73] NaPA and NaCit are carboxylic acid-rich

compounds. NaCit dissociates to provide three carboxylate ions and polyacrylic acid has one carboxylate ion per monomer.[35, 36, 72] These carboxylate ions can interact with the Ca^{2+} that resides on the crystal and the Ca^{2+} in solution, and this interaction inhibits the formation (and changes the morphology) of CaOx crystals.[36]

Thomas *et al.* studied the shape development of COD in the presence of polyacrylic acid (PAA).[70] The solution pH value and the concentration of PAA play a significant role in CaOx crystallization.[36, 70] When the pH is 2-3, the interaction between CaOx crystals and PAA is weak because PAA forms neutral chains. Thus, the growth of COM is not affected by PAA. However, at higher pH values (> 5) PAA is present as polyanionic chains that actively interact with CaOx growing crystals. This interaction prevents the formation of COM crystal and promotes the formation of COD. The inhibition of COM formation (and the promotion of COD crystallization) increases as the concentration of PAA increases. In addition, PAA causes significant changes in the morphology of growing COD crystals. Thomas *et al.* reported diverse shapes of COD crystal that formed at different pH value (6-7) and different PAA concentrations.[70]

To observe the effects of polyacrylic ions in our device, a NaPA solution of 0.5 g/L (with the pH value of 8.65) was used as the middle stream in (60, 60 mM) and (80, 80 mM) experiments. The length of the crystal line within the device decreased in comparison to the similar experiments without additives (Figures 17a and 18a). In addition, the crystal characteristics were affected; the majority of collected crystals were dumbbells[70] in the (60, 60 mM) experiments (Figure 17b and c) and rounded in the (80, 80 mM) experiments (Figure 18b and c). The rounded crystals showed a tendency to pack closely (Figure 18c). In the 60, 60 mM experiments, only dumbbells were obtained on the

collection substrate. However, SEM images of the crystal line on the PDMS revealed rounded and COD tetragonal bipyramid crystals also formed in the device (Figure 17d).

The existence of tetragonal bipyramid and rounded COD crystals in only the crystal line is probably due to the different ratio of the reagents, the velocity distribution, and the residence time within the main channel. It is possible that when the supersaturation ratio was relatively low, tetragonal bipyramids were produced. Then, as the diffusion increased with time, some of the tetragonal bipyramids transformed to dumbbells.

The ratio of CaOx and PAA in the main channel controls the morphology, which results in different shapes of COD crystals. In our device, the morphology development of COD is induced by increasing the concentration of Ca^{2+} or Ox^{2-}. In addition, the experiments described here demonstrate that dumbbells can be obtained at lower concentration than rounded; (60, 60 mM) experiments reproducibly produced dumbbells while (80, 80 mM) experiments produced rounded crystals.

A previous study has shown that at high PAA concentration dumbbells partly break along their center.[70] This trait was observed in crystals collected from the (60, 60 mM) experiments (Figure 17c). In the (80, 80 mM) experiments, it is possible that dumbbells are completely separated from their center (due to the high concentration of Ca^{2+} or Ox^{2-}) resulting in two half-rounded crystals that continued to grow into round-shaped crystals (Figure 18b and c).

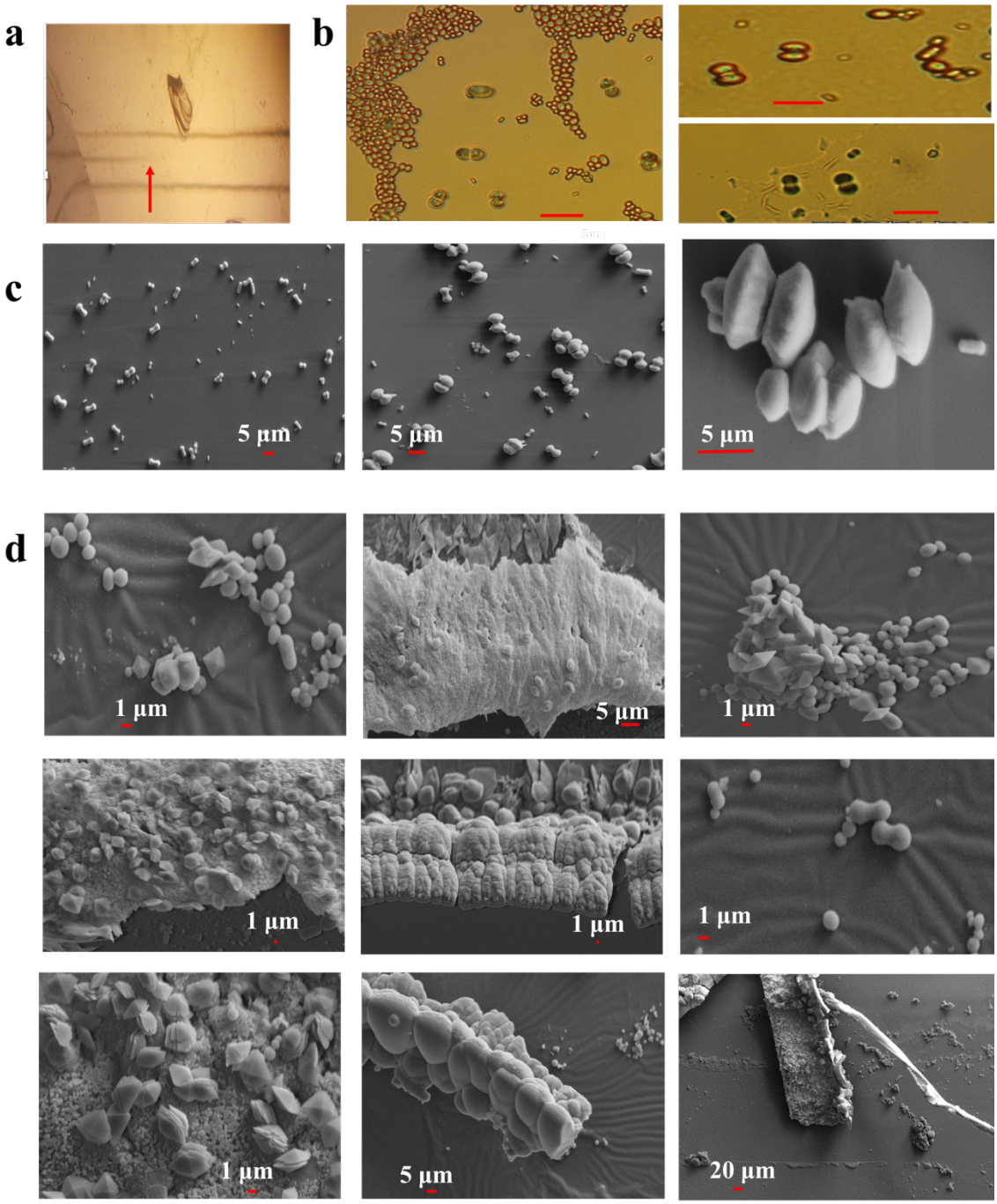

Figure 17. Optical images of (a) the crystal line and (b) CaOx crystals (with 10 µm scale bars). SEM images of (c) the collected crystals and (d) the crystal line on the PDMS. Results shown are for (60, 60 mM) experiments with 0.5 g/L of NaPA.

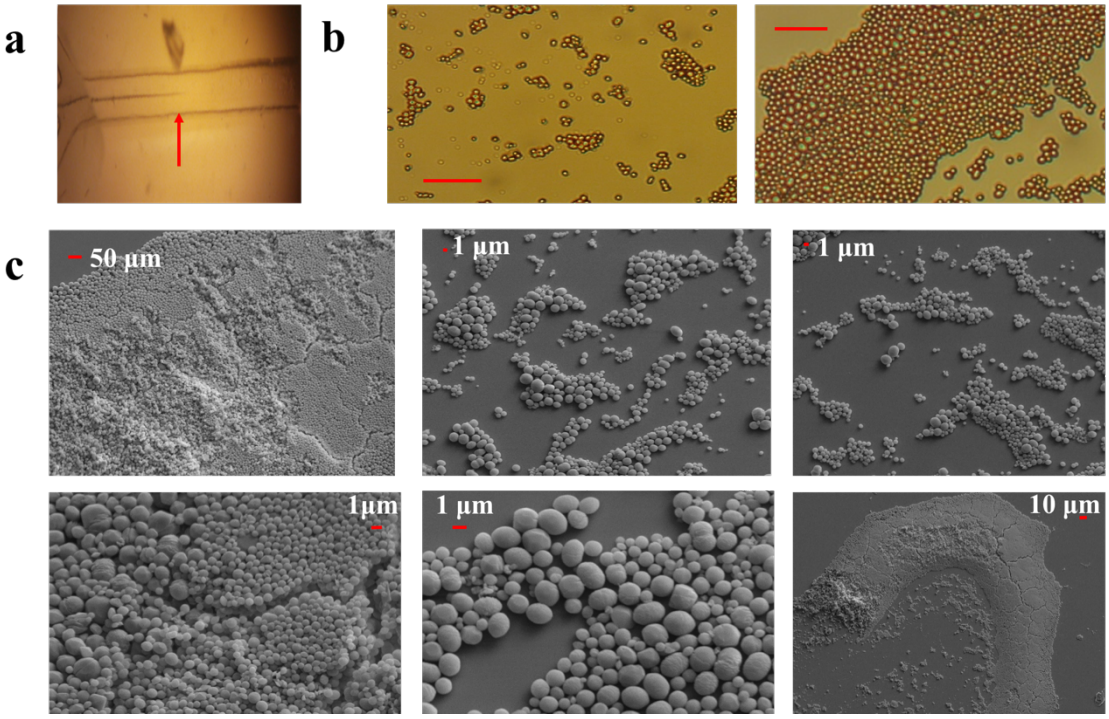

Figure 18. Optical images of (a) the crystal line and (b) CaOx crystals (with 10 µm scale bars). (c) SEM images of the collected crystals. Results shown are for (80, 80 mM) experiments with 0.5 g/L of NaPA.

As mentioned before, citrate ions can also inhibit the formation of COM. Experiments were performed using three concentrations of NaCit (50, 1, and 0.1 mM) with a non-equimolar input concentration of (80, 10 mM). For the (80, 10 mM) experiments with 50 mM of NaCit, no line was seen. Also, no crystals were observed on the collection slide. The same result was obtained using the same concentrations of Ca^{2+} and Ox^{2-} with 1 mM, and 0.1 mM of NaCit. Experiments using (80, 20 mM) with 0.1 mM of NaCit resulted in (1) a thin and light crystal line in the device (Figure 19a) and (2) only small COD crystals on the collection slide (Figure 19b). Thus, higher input concentrations of Ca^{2+} and Ox^{2-} (160, 40 mM) were used to see how this change would impact the crystal line and the CaOx morphologies. For these higher input concentrations,

the line was thicker and longer (Figure 19c). Also, large tetragonal bipyramids (and some COM) were obtained on the collection slide (Figure 19d and 19e).

No crystals were obtained when a high concentration of NaCit (50 mM) was used with input concentrations of 80 and10 mM, which suggests a significant influence of NaCit on CaOx crystallization. A high concentration of NaCit creates carboxylate ion-rich environment within the device that inhibits the formation of COM crystals. By using a high concentration of Ca^{2+}: Ox^{2-} and a relatively low concentration of NaCit (*i.e.,* 160, 40 mM with 0.1 mM NaCit), the ability of NaCit to prevent the precipitation of CaOx crystals completely was overcome.

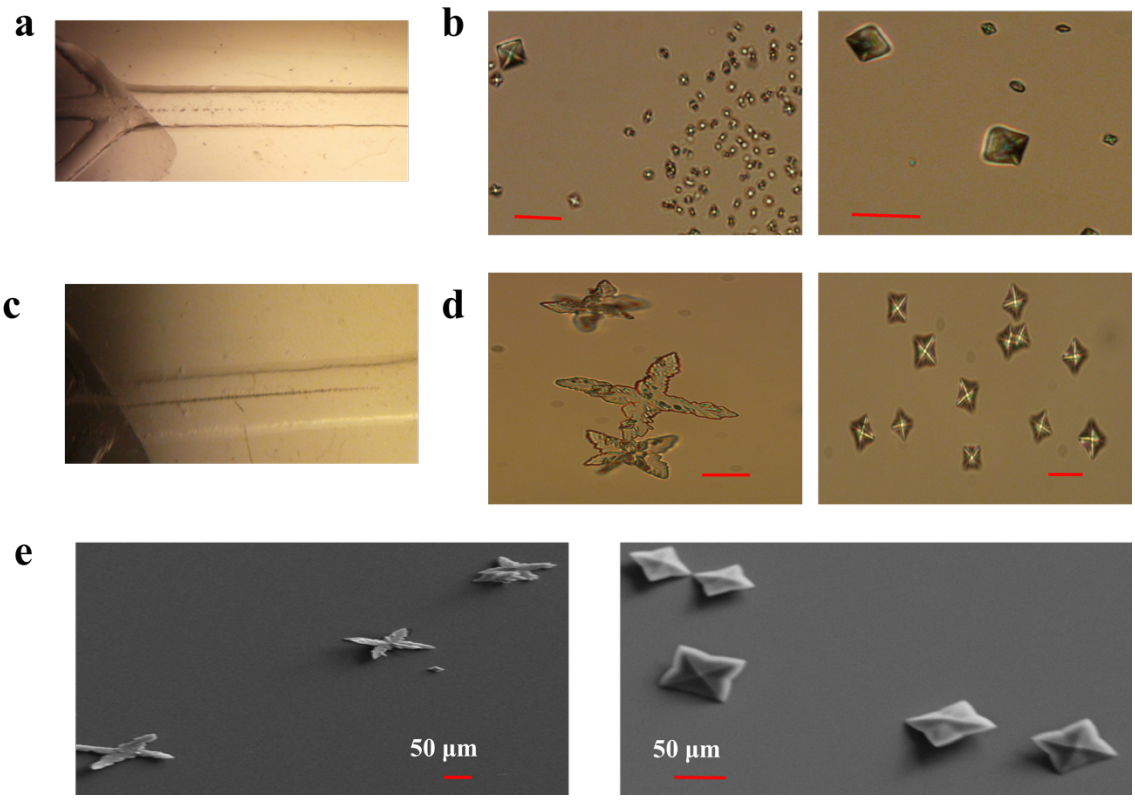

Figure 19. Optical images of (a) the line of crystal and (b) the collected crystals from (80, 20 mM) experiments with 0.1 mM of NaCit. Optical images of (c) the line of crystal and (d) the obtained crystals, and (e) SEM images from (160, 40 mM) experiments with 0.1 mM of NaCit. The scale bars of the optical images are 10 µm.

HCl was also introduced into our system as an additive to study its impact on CaOx formation. No discernable changes (compared to similar experiments without HCl) on the length of crystal line was observed when using 0.3 mM of HCl as the middle stream of (60, 60 mM) and (80, 80 mM) experiments (Figure 20a and c). However, the obtained crystals were smaller in size than those obtained without an additive. Also, more tetragonal bipyramids were collected in these experiments (Figure 20b and d).

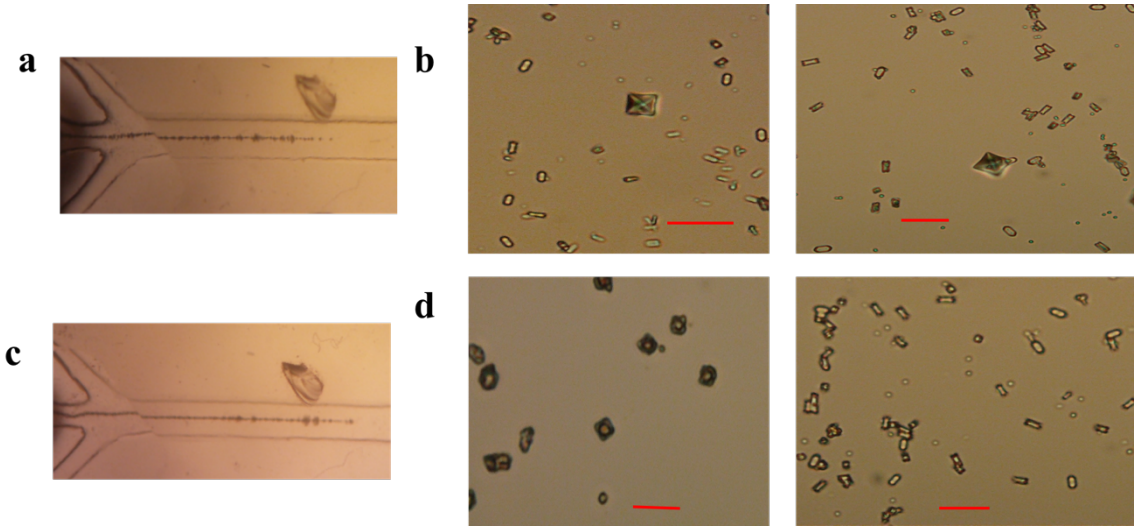

Figure 20. Optical images of (a) the line of crystal and (b) the collected crystals for (60, 60 mM) experiments with 0.3 mM of HCl. Optical images of (c) the line of crystal and (d) the obtained crystals from (80, 80 mM) experiments with 0.3 mM of HCl. The scale bars of the optical images are 10 µm.

Increasing the concentration to 1 mM HCl (in the 80, 80 mM experiments) led to changes in the crystallization process. The length of the crystal line was decreased compared to experiments using 0.3 mM of HCl (Figure 21a). The crystal line easily broke, and this is probably because the crystals were not packed together well (Figure 21b). Most of the X-shaped COM crystals that were found on the collection slide appeared to be missing a section, which suggested that CaOx crystals grown in the

presence of HCl may be more fragile (Figure 21c, the last image). Furthermore, the presence of COD was more abundant than COM crystals.

The formation of CaOx in aqueous solutions can be prevented by either reducing the oxalate or calcium ion concentrations. In our system, adding a complexing agent or chemical species shifted the chemical equilibrium of the CaOx dissolution process by involving either Ca^{2+} or Ox^{2-} in a certain chemical reaction. For instance, NaPA worked as a complexing agent that formed a complex with Ca^{2+}, and this complex inhibits the formation of CaOx crystals. Similarly, NaCit shifts the chemical equilibrium of the CaOx dissolution by reacting with Ca^{2+}, and this prevents the formation of CaOx crystals. Both NaCit and NaPA do not directly interact with the Ox^{2-}. However, by interacting with Ca^{2+} this shifts the equilibrium of CaOx dissolution process to favor the formation of Ox^{2-} and Ca^{2+}. In supersaturated solutions, the concentration of Ox^{2-} in such a system will be higher than the Ca^{2+} concentration. In contrast, the presence of HCl involves Ox^{2-} in a chemical reaction, and shifts the chemical equilibrium to produce more Ca^{2+} and Ox^{2-}; for $S > 1$ the Ca^{2+} concentration will be higher than the Ox^{2-}. This situation of having higher Ca^{2+} concentration in this system may be the cause of obtaining relatively large crystals when using HCl.

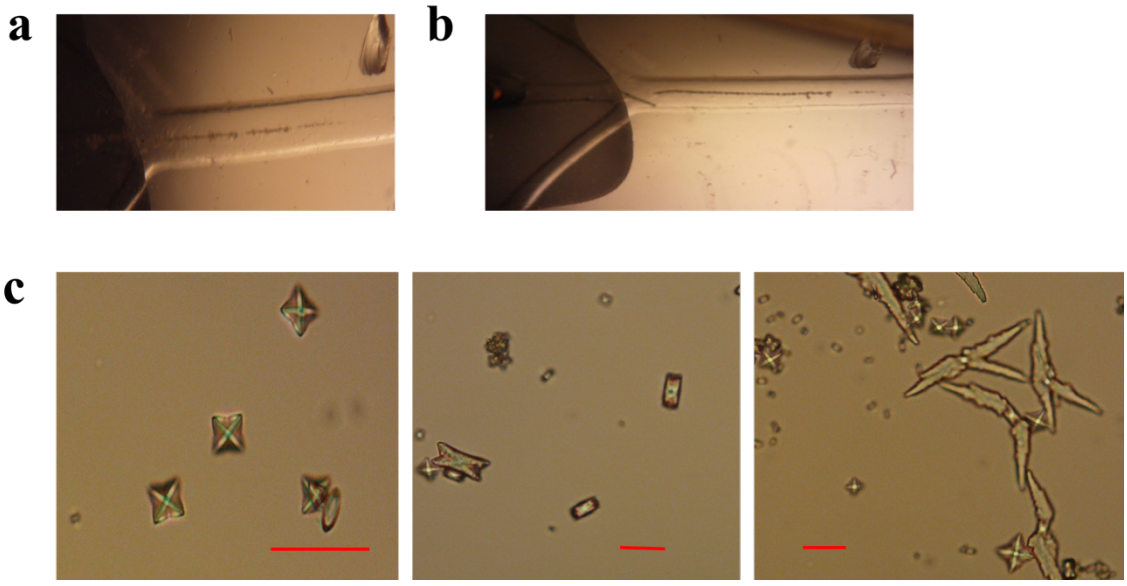

Figure 21. Optical images of (a) the line of crystal, (b) the crystal line, and (c) the collected crystals (with 10 μm scale bars) for (80, 80 mM) experiments with 1 mM of HCl.

After going carefully over all optical and SEM images of all experiments (specifically in experiments with additives), it became apparent that all obtained COD crystals were found as single crystals; meaning that COD crystals do not aggregate and stick to each other. As mentioned earlier (see section 1.2) a previous study reported that COM crystals are capable of forming stable aggregated crystals by interacting with surrounding macromolecules (in urine) that assist the formation of aggregated crystals.[18] In contrast, COD crystals were found as single crystals in voided urine. In our study, COM crystals were able to form stable aggregations even in the absence of macromolecules (Figures 13, 14 and 16).

Typically, 2 M of HCl was passed through the device to remove any crystals that remained in a device after an experiment. In (80, 80 mM) experiments in which the middle stream was 1 mM of HCl, the crystal line could be removed by flushing with distilled water. In contrast, the crystal line from other experiments (*i.e.,* equimolar

experiments with no additive) could not be removed by flushing with distilled water. Also, after observing how a high concentration of NaCit prevents the formation of CaOx, 100 mM of NaCit was used to explore the ability of NaCit to dissolve the crystal line. Flushing with a 100 mM NaCit solution through the device cleaned and dissolved the remaining crystals (*i.e.,* 160 and 40 mM experiments). However, using the solution of 1 mM HCl appeared to remove the line crystals more quickly than the 100 mM NaCit solution.

3.4 Analyzing the crystals

As other studies demonstrate, the FTIR and Raman spectra of COM crystals contain five peaks in the 2900 – 3600 cm^{-1} region. However, the spectra of COD crystals are structureless in the same region.[66, 74, 75, 76, 77] Conti *et al.* reported Raman and IR bands of COM and COD in different ranges as in Table 1.[77] Similar results were obtained when taking IR spectra of COM (commercial powder) and COD powder that was prepared following the protocol of a previous study (Figures 22 and 23).[50]

IR		Raman		Band assignments
COM	COD	COM	COD	O-H stretching
3483 m	3469 br	3486 w	3500–3200 br	
3429 m		3426 m	2941 m	
3336 m		3340 w	2855 w	
3258 m		3256 w		
3058 m		3056 m		
		2972 w		
		2919 w		
1645 sh	1640–1638 s	1629ms	1631ms	C-O stretching
1624–1622 s		1490 vs	1476 vs	
1384 w		1463 vs		
1368 w		1396ms	1416 br	
1320–1316 s	1330–1327 s			

Table 1. Raman and IR bands of COM and COD. Abbreviations used in this table (‘‘br’’ broad, ‘‘m’’ medium, ‘‘w’’ weak, ‘‘sh’’ shoulder and ‘‘s’’ strong). Data was obtained from reference 77.

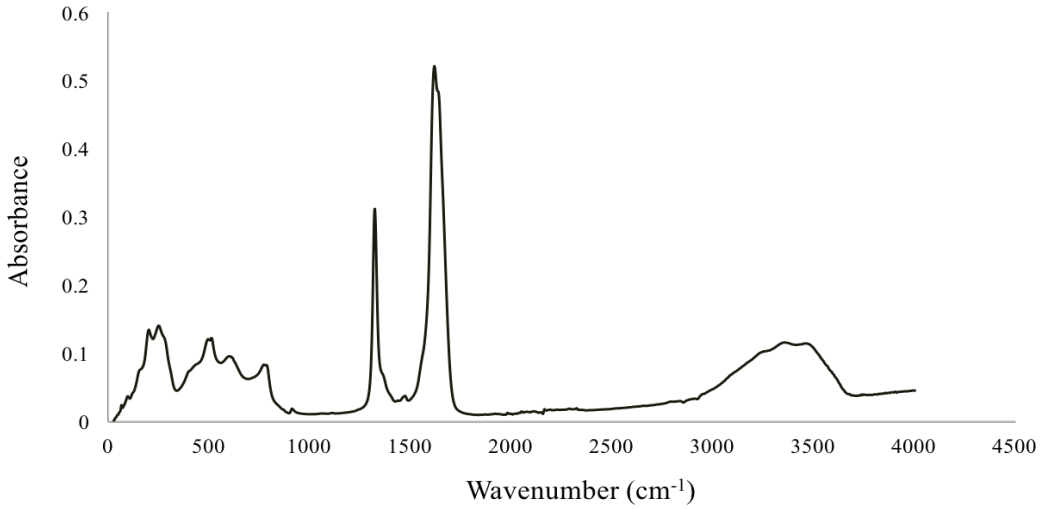

Figure 22. IR spectrum that was obtained from COD powder.

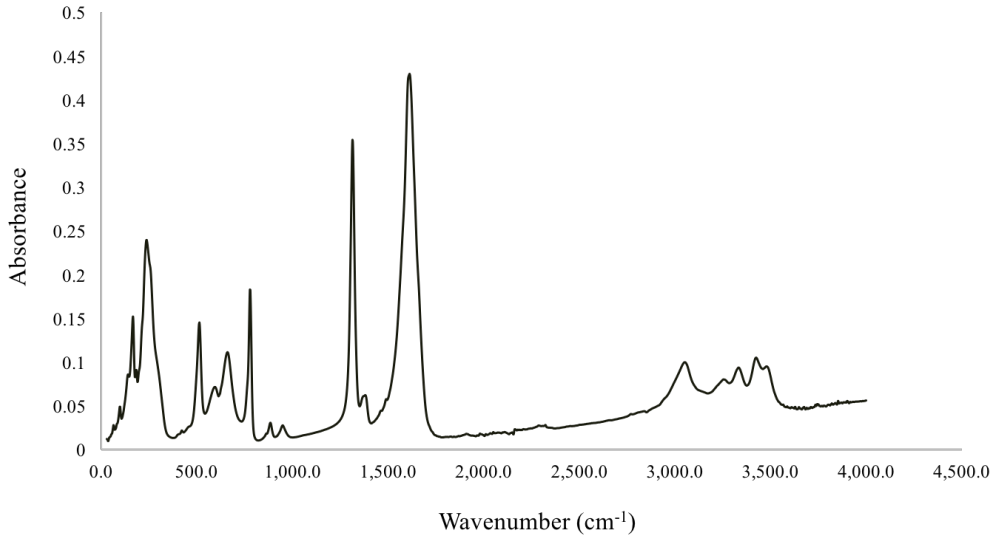

Figure 23. IR spectrum that was obtained from COM commercial powder.

The FTIR spectra obtained from our samples show that in the (20, 20 mM) experiments with no additive, the spectrum from the collected crystals has five peaks in

the 2900 – 3600 cm^{-1} region (Figure 24a). A substrate (obtained from (80, 80 mM) experiments with no additive) with an assortment of mostly COM and some COD crystals has a spectrum dominated by the spectral feature of COM (Figure 24b). A spectrum of a large X-shaped crystal (*i.e.,* 160, 40 mM experiments with 0.1 mM NaCit) contains five peaks in the 2900 – 3600 cm^{-1} region (Figure 24c). In contrast, a spectrum that was acquired from experiments with NaPA (dumbbells and roundeds) has one broad peak, suggesting the crystals are COD (Figure 24d).

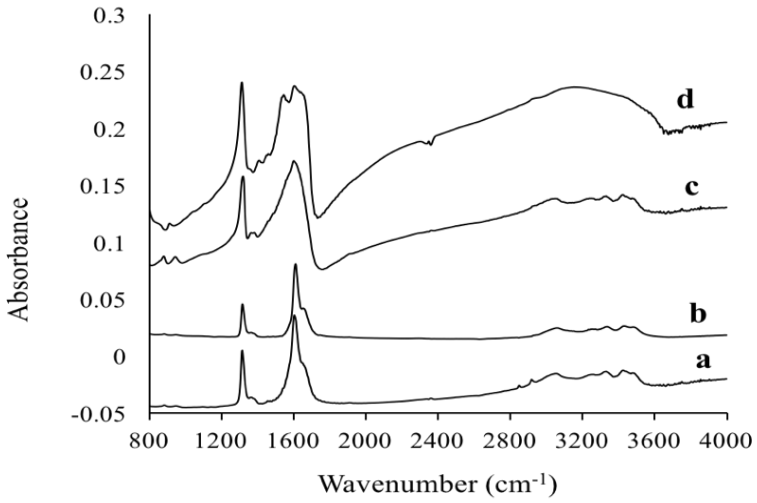

Figure 24. FTIR spectra of a crystal from (a) a (20, 20 mM) experiment, (b) a (80, 80 mM) experiment, (c) a (160, 40 mM) experiment with 0.1 mM NaCit, and (d) a (60, 60 mM) experiment with 0.5 g/L of NaPA.

By focusing on a single crystal using a confocal Raman microscope, spectra (in the 2900 – 3400 cm^{-1} region) of single crystals were obtained. The COM twin has a spectrum containing five peaks (Figure 25a). The COD dumbbell (obtained from experiments with NaPA as an additive) yields a structureless spectrum (Figure 25c). In

the experiments with NaCit, the COD tetragonal bipyramid spectrum is structureless (Figure 25d) whereas the spectrum of the X-shaped dendrites has five peaks (Figure 25b).

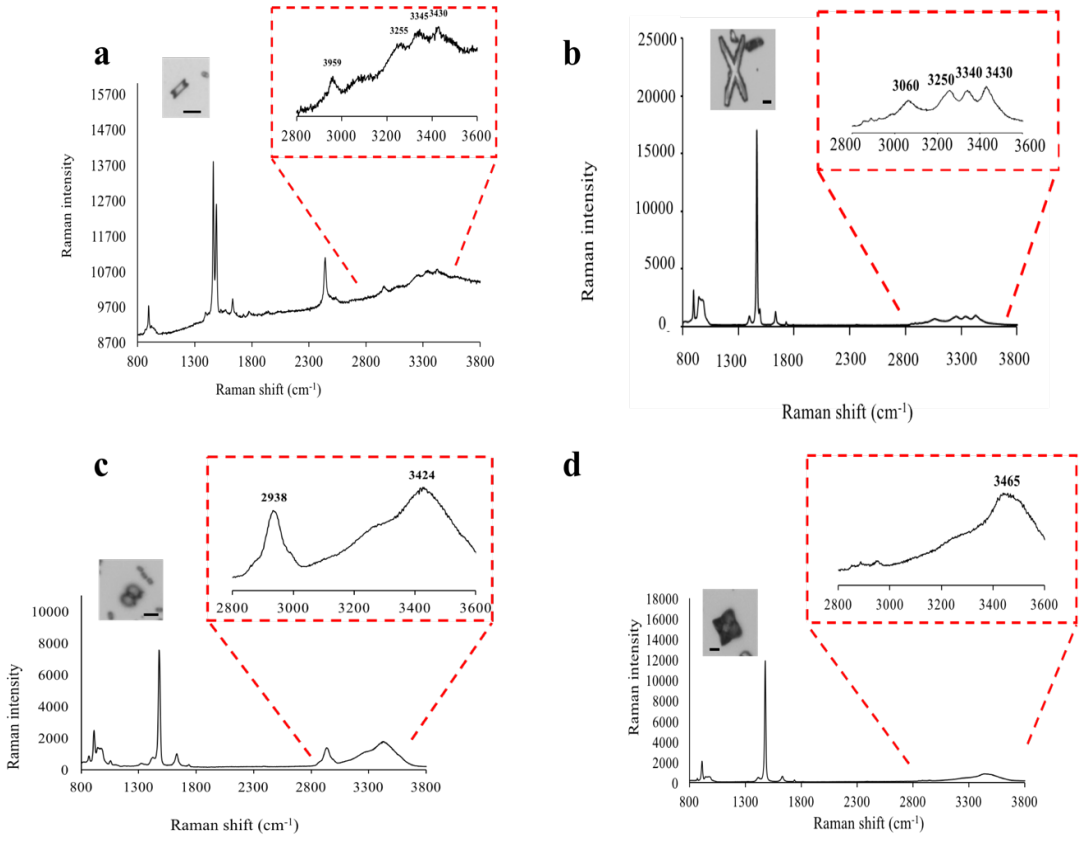

Figure 25. Raman spectra of crystals that were obtained from (a) a (20, 20 mM) experiment, (b) a (80, 80 mM) experiment, (c) a (60, 60 mM) experiment with 0.5 g/L of NaPA, and (d) a (160, 40 mM) experiment with 0.1 mM NaCit. Each spectrum, includes an expanded view of the 2900 – 3600 cm^{-1} region and an optical image of analyzed crystal.

Distinguishing CaOx crystal morphology from vibrational spectra is not always straightforward. For example, taking the spectrum of two similarly-shaped crystals (collected in experiments with NaCit) in the 2900 – 3600 cm^{-1} region showed different features; one spectrum is structureless (Figure 26a) and the other one has three peaks

(Figure 27a). Here it is difficult to distinguish if the spectrum with three peaks is COM or COD.

Determining the spectra of these two crystals in the 1400 – 1800 cm^{-1} region (C-O vibrations) is more suitable because the C-O vibrations have the highest intensity peaks in both Raman and FTIR spectra (Figures 24 and 28).[66, 77] Both crystals exhibit two peaks in the 1400 – 1550 cm^{-1} region, which suggests that these crystals are COM (Figures 26b and 27b). It was unexpected that a crystal identified based on O-H vibrations as a COD appears to be COM based on the C-O region (Figure 26b). However, this observation suggests that identifying the crystals based on the O-H vibrations may not always be accurate.

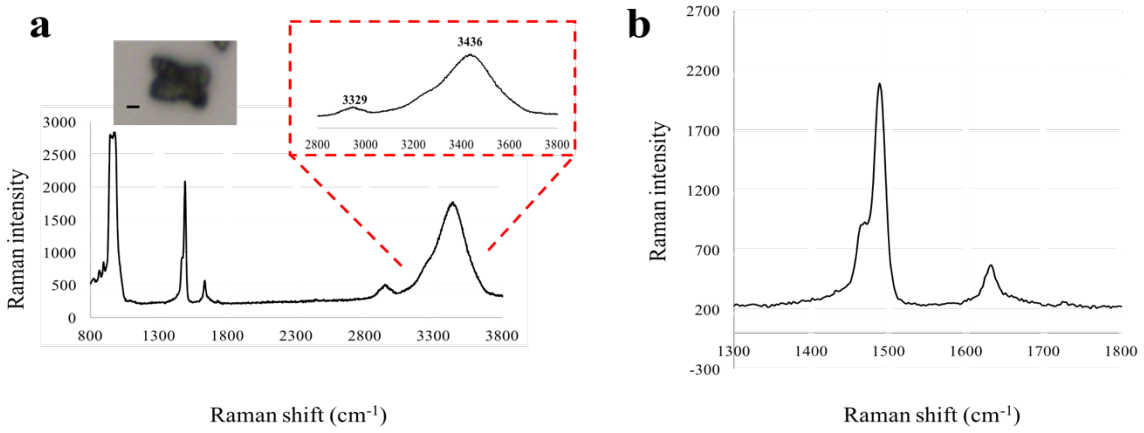

Figure 26. Raman spectra of a crystal (obtained from 160, 40 mM experiments with 0.1 mM NaCit) (a) in the 2800 – 3600 cm^{-1} region and (b) in the 1400 – 1800 cm^{-1} region.

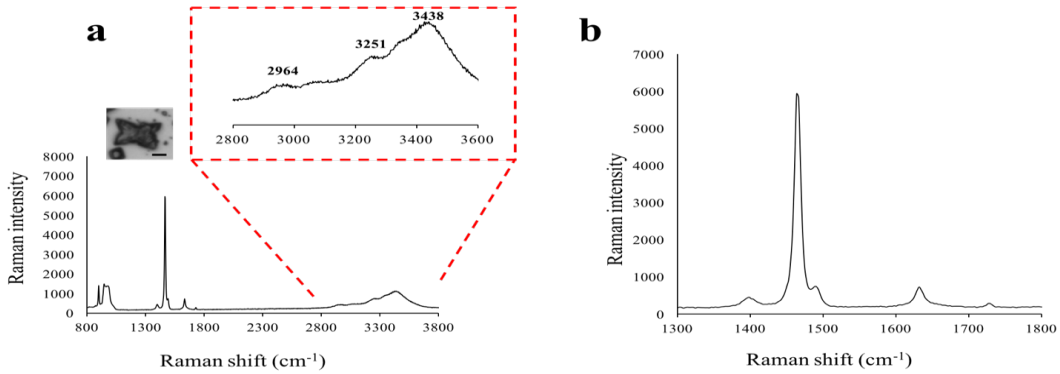

Figure 27. Raman spectra of a crystal (obtained from 160, 40 mM experiments with 0.1 mM NaCit) (a) in the 2800 – 3600 cm^{-1} region and (b) in the 1400 – 1800 cm^{-1} region.

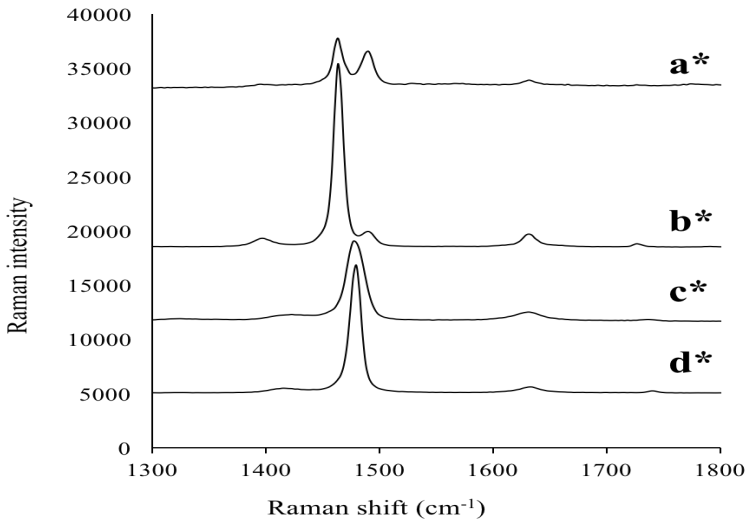

Figure 28. Raman spectra for crystals displayed in Figure 19 in the 1400 – 1800 cm^{-1} region; spectra (a*), (b*), (c*), and (d*) correspond to spectra 19a, 19b, 19c, and 19d respectively.

Even for crystals of the same morphology, the ratio of the two Raman peaks 1464 and 1490 cm^{-1} in the 1400 – 1550 cm^{-1} region is not the same for some COM crystals. In some crystals, one of the two peaks was just a shoulder. Obtaining different Raman spectra intensity for the same crystal is expected, and can be attributed to a polarization dependence of the Raman signal. To demonstrate this result further, spectra of the same COM crystal were collected using plane- polarized excitation radiation then, another

spectrum was collected using circularly polarized radiation. Figure 29 illustrates that the excitation polarization affected the intensity ratio of the two COM bands in the 1400 – 1550 cm^{-1} region. For spectra of COD crystals, which have a single band at 1479 cm^{-1}, there was no observation of a polarization dependence. This difference between the spectra of COM and COD crystals also helped to distinguish between the two crystal types.

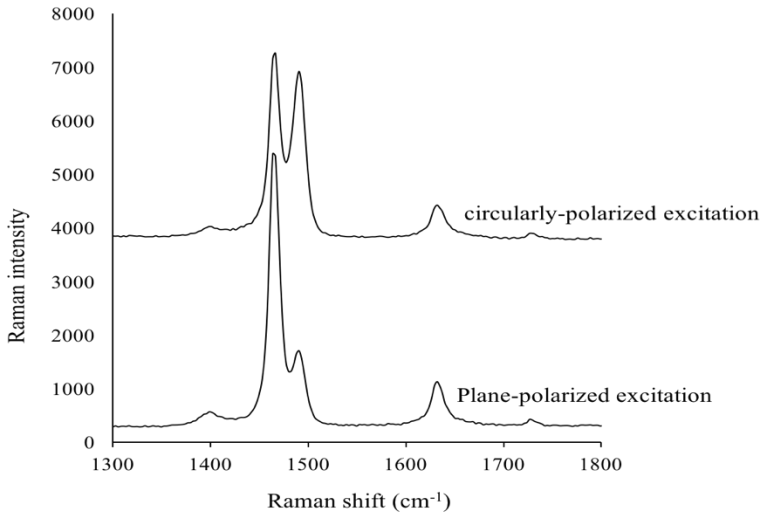

Figure 29. Raman spectra of a COM crystal in the 1400 – 1800 cm^{-1} region.

3.5. Summary

The non-droplet based microfluidic system used in this study afforded control of where crystallization took place in a device. Besides providing favorable conditions for CaOx crystallization, operational parameters were also used to eliminate the problem of crystal adhesion to the walls of a device. As far as we are aware, this is the first work involving the synthesis of CaOx crystals in a microfluidic system. Our observations reveal that crystal size and dispersity increased as the concentration of Ca^{2+} and Ox^{2-} increased. Under the same supersaturation conditions, crystals grown in a calcium-rich

environment were distinctly larger than those in an oxalate-rich environment. Therefore, the formation of large crystals can be effected by reducing Ca^{2+} concentration. As expected, the presence of carboxylate-rich compounds inhibits the formation of COM crystals. The analysis of the collected crystals using vibrational characterization method indicates that confocal Raman microscopy (which is capable of analyzing individual small crystal 1-5 μm) seems to be better suited for this study than the FTIR microscopy.

4. Future directions

This study was performed using a 2D microfluidic device that was relatively time and labor-intensive to make. The 2D device also limited this study because crystals adhering to the walls would clog the device after a critical point in crystal formation. This lowered the upper limit of concentration of Ca^{2+} and Ox^{2-} capable of being tested, as well as limiting the time an experiment could be run. Running an experiment for a long period of time is necessary when a large quantity of CaOx crystals is needed for analysis (*i.e.,* Differential scanning calorimetry (DSC) and Thermogravimetric Analysis (TGA)).

In order to further avoid crystal adhesion during CaOx crystallization, a 3D device was fabricated using a 3D printing method (as mentioned in chapter 2). The benefit of the 3D device was two-fold; it is much less time-consuming to make after printing the 3D master structure,[59, 78] and due to its 3D shape, it would not become clogged. The main difference between the 2D and 3D device is the shape of each cross-section. In the 2D device, the cross-section is a rectangle (Figure 30b), whereas the cross-section of 3D device is a cross (Figure 30a). This shape enables the crystals to form within the device without adhering to the channel wall. As shown in chapter 2, a 3D master structure was printed and molded. This mold was then cut in order to see the cross-section. Designing and printing the master structure requires working knowledge of the design program and 3D printer, and both of these proved to be barriers. Unfortunately, a second master could not be obtained due to issues relating to design and printing. However, in the future we would like to explore the possibility of using a 3D device for similar experiments.

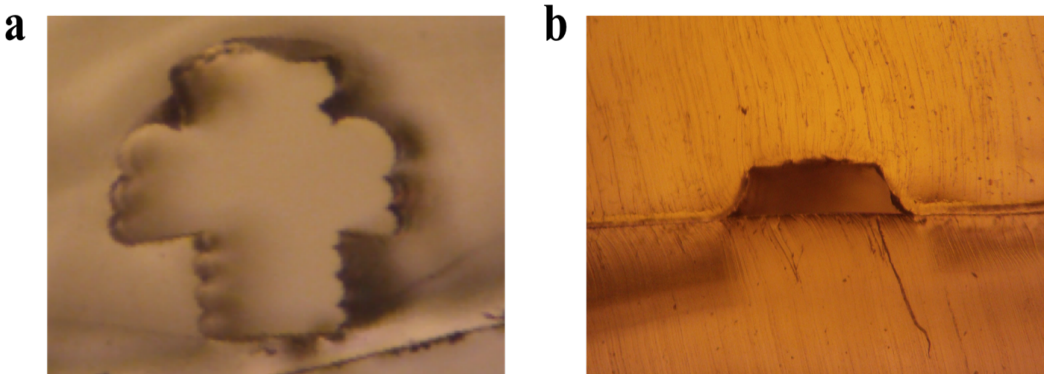

Figure 30. Optical images of the cross-section obtained from (a) a 3D microfluidic device and (b) a 2D microfluidic device.

This design can be applied to other crystallization systems (*e.g.,* $CaCO_3$, which is also found in kidney stones). There are previous studies that investigated the formation of $CaCO_3$ using droplet and non-droplet based microfluidic systems.[51, 54] However, their microfluidic systems are two inputs and one output. In addition, the influence of certain chemical species on $CaCO_3$ formation (*e.g.,* carboxylic acid compounds) was studied using different methods.[79] Therefore, $CaCO_3$ crystallization can be investigated in this system using the same strategies (*i.e.,* trying different input concentrations, equimolar and non-equimolar solutions of Ca^{2+} and CO_3^{2-}), and also the efficacy of crystallization inhibitors such as NaCit, NaPA, and HCl on the $CaCO_3$ crystallization would be useful to demonstrate. Results would then be compared to results found in the existing literature in order to see how effective our system is for the study of crystallization.

The transformation and dissolution of CaOx crystals have been highly studied.[45, 74, 80, 81] Another potential study would be to look at the effect of certain chemical species

on single crystals at certain variables such as temperature or pH. That will allow deeper insight into dissolution and transformation of CaOx.

Other chemical species such as aspartic acid, tartaric acid, malic acid, tannic acid, acetic acid, and other carboxylate-rich compounds can be examined. These species can be introduced via the middle stream to study their influence on CaOx crystallization. These carboxylate-rich compounds are naturally occurring in plants (vegetables, fruits, and herbs). Therefore, after testing the efficacy of these species *in vitro*, the next step would be applying them *in vivo*. The goal would be to see if these inhibitor compounds could be a protective agent by means of dietary supplementation. For example, in a potential study in conjunction with a kidney research center, subjects would be given dietary supplements containing different inhibiting compounds (*i.e.,* citric acid, tartaric acid) and then have their urine sampled for concentration of CaOx crystals. Samples would also by compared to control urine, to see if body metabolism and gastrointestinal absorption of these compounds will effect the concentration eventually found in urine. This study would allow us to see which compound, if any, is most efficacious *in vivo* as a dietary supplement and has the greatest potential for use as a tool in the prevention and treatment of kidney stones.

5. References

1. Myerson, A., *Handbook of industrial crystallization*. Butterworth-Heinemann: Boston, 2002.

2. Mullin, J. W., *Crystallization*. Butterworth-Heinemann: Oxford, 2001.

3. Samant, K. D.; O'Young, L., Understanding crystallization and crystallizers. *Chemical engineering progress* **2006,** *102* (10), 28-37.

4. Beckmann, W., *Crystallization: Basic Concepts and Industrial Applications*. John Wiley & Sons: Weinheim, 2013.

5. Burke, J. G., *Origins of the Science of Crystals*. Univ of California Press: Berkeley, 1966.

6. Jones, A. G., *Crystallization process systems*. Butterworth-Heinemann: Oxford, 2002.

7. Dey, A.; Bomans, P. H.; Müller, F. A.; Will, J.; Frederik, P. M.; de With, G.; Sommerdijk, N. A., The role of prenucleation clusters in surface-induced calcium phosphate crystallization. *Nature materials* **2010,** *9* (12), 1010-1014.

8. Barrett, P.; Smith, B.; Worlitschek, J.; Bracken, V.; O'Sullivan, B.; O'Grady, D., A review of the use of process analytical technology for the understanding and optimization of production batch crystallization processes. *Organic process research & development* **2005,** *9* (3), 348-355.

9. Barrett, P.; Glennon, B., In-line FBRM Monitoring of Particle Size in Dilute Agitated Suspensions. *Particle & particle systems characterization* **1999,** *16* (5), 207-211.

10. Dunuwila, D. D.; Berglund, K. A., ATR FTIR spectroscopy for in situ measurement of supersaturation. *Journal of crystal growth* **1997,** *179* (1), 185-193.

11. Lewiner, F.; Fevotte, G.; Klein, J.; Puel, F., Improving batch cooling seeded crystallization of an organic weed-killer using on-line ATR FTIR measurement of supersaturation. *Journal of crystal growth* **2001,** *226* (2), 348-362.

12. Derdour, L.; Buono, F., An Investigation of the Applicability of Microcalorimetry for the Measurement of Supersaturation during Batch Crystallization from Solution. *Crystal growth & design* **2012,** *12* (4), 1899-1912.

13. Barrett, P.; Glennon, B., Characterizing the metastable zone width and solubility curve using Lasentec FBRM and PVM. *Chemical engineering research and design* **2002,** *80* (7), 799-805.

14. Mitchell, N. A.; Frawley, P. J.; Ó'Ciardhá, C. T., Nucleation kinetics of paracetamol–ethanol solutions from induction time experiments using Lasentec FBRM®. *Journal of crystal growth* **2011,** *321* (1), 91-99.

15. Torbacke, M.; Rasmuson, Å. C., Influence of different scales of mixing in reaction crystallization. *Chemical engineering science* **2001,** *56* (7), 2459-2473.

16. Stoller, M. L.; Meng, M. V., *Urinary stone disease: the practical guide to medical and surgical management*. Springer Science & Business Media: Totowa, 2007.

17. Butts, R. E., Necessary truth in Whewell's theory of science. *American philosophical quarterly* **1965,** *2* (3), 161-181.

18. Wesson, J. A.; Ward, M. D., Pathological biomineralization of kidney stones. *Elements* **2007,** *3* (6), 415-421.

19. Bannister, F. A.; Hey, M., Report on some crystalline components of the Weddell Sea deposits. *Discovery reports* **1936,** *13*, 60-69.

20. Sayan, P.; Sargut, S. T.; Kıran, B., Calcium oxalate crystallization in the presence of amino acids, proteins and carboxylic acids. *Crystal research and technology* **2009,** *44* (8), 807-817.

21. Karas, G. V., *Focus on Crystal Growth Research*. Nova Publishers: New York, 2006.

22. Bakker, H., *Sugar cane cultivation and management*. Springer Science & Business Media: New York, 2012.

23. Maravelaki-Kalaitzaki, P., Black crusts and patinas on Pentelic marble from the Parthenon and Erechtheum (Acropolis, Athens): characterization and origin. *Analytica chimica acta* **2005,** *532* (2), 187-198.

24. Rampazzi, L.; Andreotti, A.; Bonaduce, I.; Colombini, M.; Colombo, C.; Toniolo, L., Analytical investigation of calcium oxalate films on marble monuments. *Talanta* **2004,** *63* (4), 967-977.

25. Sabbioni, C.; Zappia, G., Oxalate patinas on ancient monuments: the biological hypothesis. *Aerobiologia* **1991,** *7* (1), 31-37.

26. Polikreti, K.; Maniatis, Y., Micromorphology, composition and origin of the orange patina on the marble surfaces of Propylaea (Acropolis, Athens). *Science of the total environment* **2003,** *308* (1), 111-119.

27. Dakal, T. C.; Cameotra, S. S., Microbially induced deterioration of architectural heritages: routes and mechanisms involved. *Environmental sciences europe* **2012,** *24* (1), 1-13.

28. Eknoyan, G., History of urolithiasis. *Clinical reviews in bone and mineral metabolism* **2004,** *2* (3), 177-185.

29. Shah, J.; Whitfield, H., Urolithiasis through the ages. *BJU international* **2002,** *89* (8), 801-810.

30. Shattock, S., *A prehistoric or predynastic Egyptian calculus*. Adlard and Son: London, 1905.

31. López, M.; Hoppe, B., History, epidemiology and regional diversities of urolithiasis. *Pediatric nephrology* **2010,** *25* (1), 49-59.

32. Söhnel, O.; Grases, F., Calcium oxalate monohydrate renal calculi. Formation and development mechanism. *Advances in colloid and interface science* **1995,** *59*, 1-17.

33. Grases, F.; Gil, J.; Conte, A., Glycosaminoglycans: inhibition of calcium oxalate crystalline growth and promotion of crystal aggregation. *Colloids and surfaces* **1989,** *36* (1), 29-38.

34. Govindaraj, A.; Selvam, R., Increased calcium oxalate crystal nucleation and aggregation by peroxidized protein of human kidney stone matrix and renal cells. *Urological research* **2001,** *29* (3), 194-198.

35. Qiu, S.; Wierzbicki, A.; Orme, C.; Cody, A.; Hoyer, J.; Nancollas, G.; Zepeda, S.; De Yoreo, J., Molecular modulation of calcium oxalate crystallization by osteopontin and citrate. *Proceedings of the national academy of sciences of the United States of America* **2004,** *101* (7), 1811-1815.

36. Jung, T.; Sheng, X.; Choi, C. K.; Kim, W.-S.; Wesson, J. A.; Ward, M. D., Probing crystallization of calcium oxalate monohydrate and the role of macromolecule additives with in situ atomic force microscopy. *Langmuir* **2004,** *20* (20), 8587-8596.

37. Ramello, A.; Vitale, C.; Marangella, M., Epidemiology of nephrolithiasis. *Journal of nephrology* **2001,** *13*, 45-50.

38. Robertson, W.; Hughes, H., *Epidemiology of urinary stone disease in Saudi Arabia*. Springer: New York, 1994.

39. Sternberg, K.; Greenfield, S. P.; Williot, P.; Wan, J., Pediatric stone disease: an evolving experience. *The Journal of urology* **2005,** *174* (4), 1711-1714.

40. Robertson, W.; Peacock, M., Epidemiological factors in the genesis of calcium-containing urinary stones. *Urolithiasis* **1981**, 5-20.

41. Soucie, J. M.; Thun, M. J.; Coates, R. J.; McClellan, W.; Austin, H., Demographic and geographic variability of kidney stones in the United States. *Kidney international* **1994,** *46* (3), 893-899.

42. Asper, R., Epidemiology and socioeconomic aspects of urolithiasis. *Urological research* **1984,** *12* (1), 1-5.

43. Al-Eisa, A.; Al-Hunayyan, A.; Gupta, R., Pediatric urolithiasis in Kuwait. *International urology and nephrology* **2002,** *33* (1), 3-6.

44. Kochakarn, W.; Domrongkitchaiporn, S., Urinary risk factors for recurrent calcium stone formation in Thai stone formers. *J. Med. Assoc. Thai.* **2007,** *90* (4), 688-98.

45. Jung, T.; Kim, W.-S.; Choi, C. K., Crystal structure and morphology control of calcium oxalate using biopolymeric additives in crystallization. *Journal of crystal growth* **2005,** *279* (1), 154-162.

46. Kavanagh, J. P., In vitro calcium oxalate crystallisation methods. *Urological research* **2006,** *34* (2), 139-145.

47. Frost, R. L.; Weier, M. L., Thermal treatment of whewellite—a thermal analysis and Raman spectroscopic study. *Thermochimica acta* **2004,** *409* (1), 79-85.

48. Frost, R. L.; Weier, M. L., Thermal treatment of weddellite—a Raman and infrared emission spectroscopic study. *Thermochimica acta* **2003,** *406* (1), 221-232.

49. Akyol, E.; Öner, M., Controlling of morphology and polymorph of calcium oxalate crystals by using polyelectrolytes. *Journal of crystal growth* **2014,** *401*, 260-265.

50. Doherty, W.; Crees, O.; Senogles, E., The preparation of calcium oxalate dihydrate crystals. *Crystal research and technology* **1994,** *29* (4), 517-524.

51. Yashina, A.; Meldrum, F.; deMello, A., Calcium carbonate polymorph control using droplet-based microfluidics. *Biomicrofluidics* **2012,** *6* (2), 1-11.

52. Sultana, M.; Jensen, K. F., Microfluidic Continuous Seeded Crystallization: Extraction of Growth Kinetics and Impact of Impurity on Morphology. *Crystal growth & design* **2012,** *12* (12), 6260-6266.

53. Puigmartí-Luis, J., Microfluidic platforms: a mainstream technology for the preparation of crystals. *Chemical society reviews* **2014,** *43* (7), 2253-2271.

54. Yin, H.; Ji, B.; Dobson, P. S.; Mosbahi, K.; Glidle, A.; Gadegaard, N.; Freer, A.; Cooper, J. M.; Cusack, M., Screening of biomineralization using microfluidics. *Analytical chemistry* **2008,** *81* (1), 473-478.

55. Fujii, T., PDMS-based microfluidic devices for biomedical applications. *Microelectronic engineering* **2002,** *61*, 907-914.

56. Terry, S. C.; Jerman, J. H.; Angell, J. B., A gas chromatographic air analyzer fabricated on a silicon wafer. *Electron devices, IEEE transactions on* **1979,** *26* (12), 1880-1886.

57. Anderson, J. R.; Chiu, D. T.; Wu, H.; Schueller, O.; Whitesides, G. M., Fabrication of microfluidic systems in poly (dimethylsiloxane). *Electrophoresis* **2000,** *21* (1), 27-40.

58. Fiorini, G. S.; Chiu, D. T., Disposable microfluidic devices: fabrication, function, and application. *BioTechniques* **2005,** *38* (3), 429-446.

59. Saggiomo, V.; Velders, A. H., Simple 3D Printed Scaffold-Removal Method for the Fabrication of Intricate Microfluidic Devices. *Advanced science* **2015,** *2* (9), 1-5.

60. Femmer, T.; Kuehne, A. J.; Wessling, M., Print your own membrane: direct rapid prototyping of polydimethylsiloxane. *Lab on a chip* **2014,** *14* (15), 2610-2613.

61. Leng, J.; Salmon, J.-B., Microfluidic crystallization. *Lab on a chip* **2009,** *9* (1), 24-34.

62. Wang, Y.; Lee, D.; Zhang, L.; Jeon, H.; Mendoza-Elias, J. E.; Harvat, T. A.; Hassan, S. Z.; Zhou, A.; Eddington, D. T.; Oberholzer, J., Systematic prevention of bubble formation and accumulation for long-term culture of pancreatic islet cells in microfluidic device. *Biomedical microdevices* **2012,** *14* (2), 419-426.

63. Byrne, H.; Sockalingum, G.; Stone, N., Raman microscopy: complement or competitor. *in Moss, D. (ed.) Biomedical Applications of Synchrotron Infrared Microspectroscopy. Royal society of chemistry, RCS analytical spectroscopy monographs, no.11,* **2011**, 105-142.

64. Dieing, T.; Hollricher, O.; Toporski, J., *Confocal raman microscopy*. Springer Science & Business Media : Berlin, 2011.

65. Levin, I. W.; Bhargava, R., Fourier transform infrared vibrational spectroscopic imaging: Integrating microscopy and molecular recognition. *Annu. rev. phys. chem.* **2005,** *56*, 429-474.

66. Carmona, P.; Bellanato, J.; Escolar, E., Infrared and Raman spectroscopy of urinary calculi: A review. *Biospectroscopy* **1997,** *3* (5), 331-346.

67. Donnet, M.; Jongen, N.; Lemaitre, J.; Bowen, P., New morphology of calcium oxalate trihydrate precipitated in a segmented flow tubular reactor. *Journal of materials science letters* **2000,** *19* (9), 749-750.

68. Yu, H.; Sheikholeslami, R.; Doherty, W. O., The effects of silica and sugar on the crystallographic and morphological properties of calcium oxalate. *Journal of crystal growth* **2004,** *265* (3), 592-603.

69. Thongboonkerd, V.; Semangoen, T.; Chutipongtanate, S., Factors determining types and morphologies of calcium oxalate crystals: Molar concentrations, buffering, pH, stirring and temperature. *Clinica chimica acta* **2006,** *367* (1), 120-131.

70. Thomas, A.; Rosseeva, E.; Hochrein, O.; Carrillo-Cabrera, W.; Simon, P.; Duchstein, P.; Zahn, D.; Kniep, R., Mimicking the growth of a pathologic biomineral: shape development and structures of calcium oxalate dihydrate in the presence of polyacrylic acid. *Chemistry–A european journal* **2012,** *18* (13), 4000-4009.

71. Pak, C., Citrate and renal calculi: an update. *Mineral and electrolyte metabolism* **1993,** *20* (6), 371-377.

72. Lee, T.; Lin, Y. C., Mimicking the initial development of calcium urolithiasis by screening calcium oxalate and calcium phosphate phases in various urinelike solutions, time points, and pH values at 37 C. *Crystal growth & design* **2011,** *11* (7), 2973-2992.

73. Basavaraj, D. R.; Biyani, C. S.; Browning, A. J.; Cartledge, J. J., The role of urinary kidney stone inhibitors and promoters in the pathogenesis of calcium containing renal stones. *EAU-EBU update series* **2007,** *5* (3), 126-136.

74. Conti, C.; Casati, M.; Colombo, C.; Realini, M.; Brambilla, L.; Zerbi, G., Phase transformation of calcium oxalate dihydrate–monohydrate: Effects of relative humidity and new spectroscopic data. *Spectrochimica Acta Part A: Molecular and biomolecular spectroscopy* **2014,** *128*, 413-419.

75. Conti, C.; Brambilla, L.; Colombo, C.; Dellasega, D.; Gatta, G. D.; Realini, M.; Zerbi, G., Stability and transformation mechanism of weddellite nanocrystals studied by X-ray diffraction and infrared spectroscopy. *Physical chemistry chemical physics* **2010,** *12* (43), 14560-14566.

76. Pinales, L.; Chianelli, R.; Durrer, W.; Pal, R.; Narayan, M.; Manciu, F., Spectroscopic study of inhibition of calcium oxalate calculi growth by Larrea tridentata. *Journal of raman spectroscopy* **2011,** *42* (3), 259-264.

77. Conti, C.; Casati, M.; Colombo, C.; Possenti, E.; Realini, M.; Gatta, G. D.; Merlini, M.; Brambilla, L.; Zerbi, G., Synthesis of calcium oxalate trihydrate: New data by vibrational spectroscopy and synchrotron X-ray diffraction. *Spectrochimica Acta Part A: Molecular and biomolecular spectroscopy* **2015,** *150*, 721-730.

78. Erkal, J. L.; Selimovic, A.; Gross, B. C.; Lockwood, S. Y.; Walton, E. L.; McNamara, S.; Martin, R. S.; Spence, D. M., 3D printed microfluidic devices with integrated versatile and reusable electrodes. *Lab on a chip* **2014,** *14* (12), 2023-2032.

79. Wada, N.; Kanamura, K.; Umegaki, T., Effects of carboxylic acids on the crystallization of calcium carbonate. *Journal of colloid and interface science* **2001,** *233* (1), 65-72.

80. Brečević, L.; Škrtić, D.; Garside, J., Transformation of calcium oxalate hydrates. *Journal of crystal growth* **1986,** *74* (2), 399-408.

81. Sikirić, M.; Filipović-Vinceković, N.; Babić-Ivančić, V.; Vdović, N.; Füredi-Milhofer, H., Interactions in calcium oxalate hydrate/surfactant systems. *Journal of colloid and interface science* **1999,** *212* (2), 384-389.